U.S. Department
of Transportation

Federal Railroad
Administration

Office of Research,
Development and Technology
Washington, DC 20590

NDE Methods for Corrosion Monitoring in Railroad Tank Cars

DOT/FRA/ORD-23/03

Final Report | January 2023

REPORT DOCUMENTATION PAGE						*Form Approved* *OMB No. 0704-0188*
The public reporting burden for this collection of information is estimated to average 1 hour per response, including the time for reviewing instructions, searching existing data sources, gathering and maintaining the data needed, and completing and reviewing the collection of information. Send comments regarding this burden estimate or any other aspect of this collection of information, including suggestions for reducing the burden, to Department of Defense, Washington Headquarters Services, Directorate for Information Operations and Reports (0704-0188), 1215 Jefferson Davis Highway, Suite 1204, Arlington, VA 22202-4302. Respondents should be aware that notwithstanding any other provision of law, no person shall be subject to any penalty for failing to comply with a collection of information if it does not display a currently valid OMB control number. **PLEASE DO NOT RETURN YOUR FORM TO THE ABOVE ADDRESS.**						
1. REPORT DATE *(DD-MM-YYYY* January 2023		**2. REPORT TYPE** Technical Report				**3. DATES COVERED** *(From - To)* October 1, 2018–July 30, 2022
4. TITLE AND SUBTITLE NDE Methods for Corrosion Monitoring in Railroad Tank Cars						**5a. CONTRACT NUMBER** DTFR53-11-D-00008L
						5b. GRANT NUMBER
						5c. PROGRAM ELEMENT NUMBER
6. AUTHOR(S) Anish Poudel – 0000-0002-5811-4284 Brian Lindeman – 0000-0003-3903-266X Survesh Shrestha – 0000-0002-2070-748X Kenny Morrison – 0000-0003-1382-4175						**5d. PROJECT NUMBER**
						5e. TASK NUMBER 693JJ618F000067
						5f. WORK UNIT NUMBER
7. PERFORMING ORGANIZATION NAME(S) AND ADDRESS(ES) Transportation Technology Center, Inc. 55500 DOT Road Pueblo, CO 81001-0130						**8. PERFORMING ORGANIZATION REPORT NUMBER**
9. SPONSORING/MONITORING AGENCY NAME(S) AND ADDRESS(ES) U.S. Department of Transportation Federal Railroad Administration Office of Railroad Policy and Development Office of Research, Data and Innovation Washington, DC 20590						**10. SPONSOR/MONITOR'S ACRONYM(S)**
						11. SPONSOR/MONITOR'S REPORT NUMBER(S) DOT/FRA/ORD-23/03
12. DISTRIBUTION/AVAILABILITY STATEMENT This document is available to the public through the FRA website.						
13. SUPPLEMENTARY NOTES COR: Francisco González, III						
14. ABSTRACT This report discusses the use of various nondestructive evaluation (NDE) methods for detecting and characterizing corrosion defects in tank cars. Several tank car panels with a real corrosion defect as well as simulated corrosion defects were fabricated from the actual tank car. Advanced NDE methods such as Phased Array Ultrasonic Testing, Electromagnetic Acoustic Transducers, backscatter X-ray imaging, and three-dimensional laser scanning metrology were explored on the test panels. While these NDE methods demonstrated good feasibility, further efforts should be considered and explored in a more systematic way that will allow for a better understanding of the capabilities and limitations of these NDE methods. Also, future efforts should consider building more test panels for the corrosion NDE demonstration.						
15. SUBJECT TERMS Tank cars, corrosion, pitting, fatigue, master gauge, MG, nondestructive evaluation, NDE, ultrasonic testing, UT, Phased Array Ultrasonic Testing, PAUT, Electromagnetic Acoustic Transducers, EMAT, Backscatter X-ray imaging, 3D laser scanning metrology, hazardous materials						
16. SECURITY CLASSIFICATION OF:			**17. LIMITATION OF ABSTRACT**	**18. NUMBER OF PAGES**	**19a. NAME OF RESPONSIBLE PERSON** Francisco González, III	
a. REPORT Unclassified	**b. ABSTRACT** Unclassified	**c. THIS PAGE** Unclassified		86	**19b. TELEPHONE NUMBER** *(Include area code)* 202-493-6076	

Standard Form 298 (Rev. 8/98)
Prescribed by ANSI Std. Z39.18

METRIC/ENGLISH CONVERSION FACTORS

ENGLISH TO METRIC

LENGTH (APPROXIMATE)

1 inch (in)	=	2.5 centimeters (cm)
1 foot (ft)	=	30 centimeters (cm)
1 yard (yd)	=	0.9 meter (m)
1 mile (mi)	=	1.6 kilometers (km)

AREA (APPROXIMATE)

1 square inch (sq in, in^2)	=	6.5 square centimeters (cm^2)
1 square foot (sq ft, ft^2)	=	0.09 square meter (m^2)
1 square yard (sq yd, yd^2)	=	0.8 square meter (m^2)
1 square mile (sq mi, mi^2)	=	2.6 square kilometers (km^2)
1 acre = 0.4 hectare (he)	=	4,000 square meters (m^2)

MASS - WEIGHT (APPROXIMATE)

1 ounce (oz)	=	28 grams (gm)
1 pound (lb)	=	0.45 kilogram (kg)
1 short ton = 2,000 pounds (lb)	=	0.9 tonne (t)

VOLUME (APPROXIMATE)

1 teaspoon (tsp)	=	5 milliliters (ml)
1 tablespoon (tbsp)	=	15 milliliters (ml)
1 fluid ounce (fl oz)	=	30 milliliters (ml)
1 cup (c)	=	0.24 liter (l)
1 pint (pt)	=	0.47 liter (l)
1 quart (qt)	=	0.96 liter (l)
1 gallon (gal)	=	3.8 liters (l)
1 cubic foot (cu ft, ft^3)	=	0.03 cubic meter (m^3)
1 cubic yard (cu yd, yd^3)	=	0.76 cubic meter (m^3)

TEMPERATURE (EXACT)

[(x-32)(5/9)] °F = y °C

METRIC TO ENGLISH

LENGTH (APPROXIMATE)

1 millimeter (mm)	=	0.04 inch (in)
1 centimeter (cm)	=	0.4 inch (in)
1 meter (m)	=	3.3 feet (ft)
1 meter (m)	=	1.1 yards (yd)
1 kilometer (km)	=	0.6 mile (mi)

AREA (APPROXIMATE)

1 square centimeter (cm^2)	=	0.16 square inch (sq in, in^2)
1 square meter (m^2)	=	1.2 square yards (sq yd, yd^2)
1 square kilometer (km^2)	=	0.4 square mile (sq mi, mi^2)
10,000 square meters (m^2)	=	1 hectare (ha) = 2.5 acres

MASS - WEIGHT (APPROXIMATE)

1 gram (gm)	=	0.036 ounce (oz)
1 kilogram (kg)	=	2.2 pounds (lb)
1 tonne (t)	=	1,000 kilograms (kg)
	=	1.1 short tons

VOLUME (APPROXIMATE)

1 milliliter (ml)	=	0.03 fluid ounce (fl oz)
1 liter (l)	=	2.1 pints (pt)
1 liter (l)	=	1.06 quarts (qt)
1 liter (l)	=	0.26 gallon (gal)
1 cubic meter (m^3)	=	36 cubic feet (cu ft, ft^3)
1 cubic meter (m^3)	=	1.3 cubic yards (cu yd, yd^3)

TEMPERATURE (EXACT)

[(9/5) y + 32] °C = x °F

QUICK INCH - CENTIMETER LENGTH CONVERSION

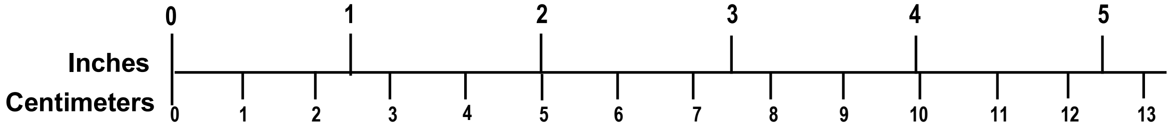

QUICK FAHRENHEIT - CELSIUS TEMPERATURE CONVERSIO

°F	-40°	-22°	-4°	14°	32°	50°	68°	86°	104°	122°	140°	158°	176°	194°	212°
°C	-40°	-30°	-20°	-10°	0°	10°	20°	30°	40°	50°	60°	70°	80°	90°	100°

For more exact and or other conversion factors, see NIST Miscellaneous Publication 286, Units of Weights and Measures. Price $2.50 SD Catalog No. C13 10286 **Updated 6/17/98**

Acknowledgements

The authors would like to thank the team members and industry participants who supported this work. Special thanks to Boeing Research & Technology in Seattle, WA, Innerspec Inc., and Creaform for their support in conducting the various measurements in this study.

Contents

Illustrations

Tables

Executive Summary

As part of the ongoing tank car research program, the Federal Railroad Administration contracted Transportation Technology Center, Inc. (TTCI) to investigate both the issues of corrosion on railway tank cars and in other industries and the nondestructive evaluation (NDE) technologies to characterize corrosion defects. From October 2018 through July 2022, the research team performed the following tasks: 1) summarizing the findings, 2) describing the NDE methods currently used for measuring and evaluating corrosion, and 3) providing a high-level overview of the related issues of corrosion formation and mitigation. This research also looks forward to new NDE methodologies for characterizing corrosion in railway tank cars by surveying and inspecting several U.S. Department of Transportation (DOT) tank cars (retired cars or donated cars for other testing purposes) at the Transportation Technology Center (TTC) in Pueblo, CO. Based on the observations, it can be concluded that some of the tank cars demonstrated different levels of corrosion both on the inner diameter (ID) and outer diameter (OD). In some of the jacketed tank cars, the OD and ID corrosion was severe in the metal jackets used in some DOT tank cars.

Some industry professions took a short survey to understand the challenges associated with corrosion in the existing tank car fleets. Based on discussions, these industry professionals determined that the area of corrosion inside the tank car primarily depends on the material that the tank car transports. Acids and chlorine typically cause corrosion in a band around the top of the tank car at the 10:00 and 2:00 o'clock positions. Crude oil, with heavy sediments, typically causes corrosion in a band along the bottom of the tank car at the 5:00 and 7:00 o'clock positions. Corrosion can also occur in areas such as the nozzle body or near valves. Sodium bisulfite and ammonium nitrate are solid catalysts for corrosion, and both tend to attack unprotected metal anywhere they encounter.

Researchers surveyed tank cars at the TTC. Those that presented some amounts of corrosion were selected for developing several test panels that were cut out of the tank cars. In addition, master gauge plates, consisting of defined size simulated corrosion and pit defects in the ID and OD of the DOT-117 tank car shells, were fabricated. In addition, another set of test samples consisting of three different tank car reflector plates was fabricated from one DOT-117 tank car shell. These plates consisted of varied size (diameter and depth) holes drilled on the surface of these plates.

Some of the advanced NDE methods explored as a part of this study included Phased Array Ultrasonic Testing (PAUT), electromagnetic acoustic transducers (EMATs), backscatter X-ray imaging, and three-dimensional laser scanning metrology methods. While these NDE methods demonstrated good feasibility, further efforts should be considered and pursued in exploring each of these and other NDE methods in a more systematic way to better understand the capabilities and limitations of each NDE methods. Future efforts should also consider building more test panels for the corrosion NDE demonstration.

1. Introduction

From October 2018 to July 2022, the Federal Railroad Administration (FRA) contracted Transportation Technology Center, Inc. (TTCI) to investigate the types of corrosion common on railroad tank cars. Corrosion detection also explores the possible advanced nondestructive evaluation (NDE) methods for facilitating the measurement and evaluation of the corrosion in tank cars.

The primary structure of modern railroad tank cars, including the inner shell, is made of fine-grain heat-treated steel and incorporates various safety features to improve the cars' puncture resistance. However, these steel tank car structures are still prone to corrosion over time, and when advanced, corrosion weakens the metal and can lead to material failure if not mitigated. Corrosion is the natural process of metal deterioration that restores the refined metal to its chemically stable form. It results from the interaction of the metal with its environment or the commodities (e.g., chemicals that include acids, chlorine, ammonia, ethanol, and crude oil) it carries and is difficult to prevent entirely. Corrosion can be a significant factor that limits the life of tank cars. Tank car corrosion often forms in concealed locations and can remain hidden until it reaches advanced stages. Corrosion detection through better inspection practices is necessary for effective preventative maintenance and mitigation strategies.

1.1 Background

The first oil tank cars built in the 1860s consisted of wood vats on a flat car. The wood vats were prone to leaking, and their capacity was limited by height and width restrictions. By the late 1860s, the design changed to a horizontal boiler-type configuration made from iron. Figure 1 shows examples of early tank car designs.

(a) (b)

Figure 1. First tank car designs from the 1860s and 1880s

The horizontal configuration of these early tank cars resembles the modern design. The tank size increased from 3,400 gallons in the original tank cars to over 30,000 gallons in today's modern tank cars. The advanced steel designs and material properties allowed for longer life and additional excellent corrosion prevention opportunities.

Specifications for railroad tank cars first appeared in a report to the former Master Car Builders' Association in 1903 [1]. The American Railway Association in 1925 approved, revised, and issued this report with specification adoption on March 1, 1931, by the Association of American Railroads (AAR). On July 1, 1927, Interstate Commerce Commission (ICC) specifications were issued for tank car transportation of articles classified as dangerous by ICC regulations, and AAR specifications for such tanks became obsolete. ICC regulations were then published and revised as a part of Title 49 Code of Federal Regulations (CFR). After the passage of the Department of Transportation Act in October 1966, these regulations became the U.S. Department of Transportation's (DOT) Hazardous Materials Regulations (HMR), effective April 1, 1967. The HMR is currently included in CFR Title 49 Parts 179–180, Subtitle B–Other Regulations Relating to Transportation, Chapter I–Pipeline and Hazardous Materials Safety Administration, Department of Transportation, Subchapter C–Hazardous Materials Regulations[2]. Also, the AAR Manual of Standards and Recommended Practices (MSRP), Section C, Part III, Specifications for Tank Cars [3], provides specifications for tank cars transporting "dangerous" commodities (or hazardous materials [HazMat]), and tanks for commodities not classified as HazMat and consequently subject only to AAR regulations.

1.2 Objectives

The goal of the tank car NDE research program is to advance tank car safety by ensuring structural integrity. The primary objective of the work reported in this report is 1) to facilitate the understanding of different types of corrosion common on railroad tank cars, 2) to investigate the effect of each type of corrosion on tank car structural integrity, and 3) to explore the application of advanced NDE methods for measuring and evaluating tank car corrosion.

1.3 Overall Approach

To understand the composition of the current tank car fleet in service, this research included:

- An extensive literature review.
- A focus on understanding the underlying root cause of corrosion in tank cars in service and the effect of corrosion on tank car structural integrity.
- An exploration of the inspection practices currently employed by the railroad industry to monitor the corrosion in tank cars and by other industries such as pipeline and nuclear to monitor the corrosion for their applications.
- An attempt to create smaller tank car corroded panels from corroded tank cars, characterize them, and conduct the feasibility of applying some of the advanced NDE methods for tank car corrosion.

1.4 Scope

This research explored some advanced NDE methods as part of this study that includes Phased Array Ultrasonic Testing (PAUT), electromagnetic acoustic transducers (EMATs), backscatter X-ray imaging, and three-dimensional (3D) laser scanning metrology methods. It should be identified if these NDE methods demonstrate good feasibility to detect the corrosion on tank cars.

1.5 Organization of the Report

This report is organized as follows:

- Section 1 introduces the research conducted and provides an overview.
- Section 2 provides a general background on the railroad tank cars, their designs, and constructions based on the commodities they carry.
- Section 3 encloses the general corrosion overview and typical corrosion issues in different tank cars. It also describes current best practices by railroad industries and other industries, such as oil, gas, pipeline and nuclear, to monitor corrosion in their applications.
- Section 4 provides some of the early initiatives that the research team took to create smaller tank car corroded panels from corroded tank cars, characterize them, and conduct the feasibility study of applying some of the advanced NDE methods for tank car corrosion.
- Section 5 details the development of the corrosion test panels.
- Section 6 describes the NDE trials for corrosion assessment in the corrosion test panels.
- Section 7 summarizes the findings and provides recommendations for future work.

2. Railroad Tank Cars

Railroad tank cars in North America haul different commodities ranging from food products to clay slurry, chemicals, and crude oil, which are all essential products to consumers and markets. There are mainly two general commodities transported via rail: "non-regulated" or "non-hazardous" and "hazardous" materials. Tank cars hauling these commodities in North American railroads are classified as three types: DOT, AAR, and ICC. Tank cars used for transporting HazMat must comply with DOT specifications. With a few exceptions, AAR-specification tanks are used to transport materials not classified as hazardous by DOT. In general, ICC tank car specifications are re-designed DOT specifications.

A DOT tank car specification number consists of a class designation followed by identifying letters and numbers. Except for 103, 104, and 113, the class designation is followed by an "A," which has no special significance. The suffix "W" denotes a fusion-welded tank; suffix "F" denotes a forge-welded tank; and suffix "X" has special significance regarding how tank cars are constructed. The absence of a suffix indicates seamless tank construction.

All car structure details must comply with both AAR specifications and related specifications, and publications listed in AAR MSRP Specification M-1001, Paragraph 1.1.2 [4]. Most AAR tank cars have DOT and Transport Canada (TC) counterparts, with the leading specification differences related to heat treating and weld inspection requirements. As with DOT tank cars, the suffix "W" denotes a fusion-welded tank.

The AAR tank cars that are not re-designated have riveted or forge-welded tanks but conform to corresponding DOT classes in other respects. All tanks and appurtenances constructed for use in transporting materials classified as hazardous by DOT must comply with the applicable DOT specifications and additional AAR requirements. Therefore, the DOT specifications for tanks and equipment are general and minimum. AAR-specification tanks are used for transporting materials not classified as hazardous by DOT, except that certain low- and medium-hazard materials are permitted in AAR-specification tanks as described in 49 CFR Sections 173.240, 173.241, and 173.242 [2]. Such tanks and appurtenances must comply with all applicable AAR specifications and requirements in effect at the time of construction.

2.1 Tank Cars in Service

The North American tank car fleet consists of about 433,000 tank cars, and this accounts for 27 percent of the total railcar fleet [5]. In North America, tank cars are grouped by type and not by the cargo carried. Tank cars carrying HazMat are generally constructed from different types of materials and configurations, depending on the intended cargo and operating pressure. Table 1 lists the descriptions of some common types of tank cars currently in service in North American railroads. A detailed description of these tank cars can also be found in outside literature [3]. Non-pressurized tank cars are also known as general service tank cars, and they carry a variety of HazMat and non-HazMat commodities at pressures normally below 25 psi. However, pressurized tank cars are built with a protective housing, and these cars typically carry flammable, non-flammable, toxic, and/or liquefied compressed gases at pressures usually above 40 psi. Similarly, cryogenic tank cars are used for the transportation of super-cold cryogenic fluids such as liquified oxygen, nitrogen, and argon over long distances.

Table 1. List of tank cars currently used in North American railroads

Type	Meaning
	Non-Pressurized Designations
DOT-103	Non-pressure, insulated or non-insulated, with expansion dome (built for specific services or requiring special fittings or construction materials)
AAR-203	Non-pressure, non-insulated with an expansion dome. These cars conform, with certain exceptions, to Class DOT-103W.
DOT-104	Non-pressure, insulated, with expansion dome
DOT-111	Insulated or non-insulated, without an expansion dome. The shell is 7/16-inch thick.
AAR-211	Insulated or non-insulated, without an expansion dome. These cars conform, with certain exceptions, to Class DOT-11A***W*.
AAR CPC-1232	Include a pressure relief valve, more extensive top fittings than on the DOT-111 rail tank cars, and a full height or half-height head shield. The shell of non-jacketed tank cars must be 1/2-inch thick, and for jacketed tank cars must be 7/16-inch thick.
DOT-115	Insulated with a carbon or alloy (stainless) steel or an aluminum inner container (tank) and a carbon steel outer shell (tank, not jacket). Otherwise known as a tank within a tank; AAR-206W cars conform, with certain exceptions, to Class DOT-115A***W*.
DOT-117	Insulated with a carbon steel (minimum 11 gauge) and thermal protection. The shell is 9/16-inch thick.
DOT-206	Insulated with an inner-container (tank) and carbon steel outer-shell. Similar to DOT-115.
DOT-211	Insulated or non-insulated, without an expansion dome. Similar to DOT-111.
	Pressurized Designations
DOT-105	Insulated carbon or alloy steel with a manway nozzle
DOT-107	Non-insulated cars having several permanently mounted seamless, forged, and drawn steel tanks designed to a maximum stress level in the shell
DOT-109	Insulated or non-insulated, carbon steel or aluminum alloy with a manway nozzle, designed for top loading and unloading, bottom washout optional. AAR-205A300W tank cars are now designated DOT-109A300W.
DOT-112	Insulated or non-insulated, carbon or alloy steel with a manway nozzle and without bottom connections, designed for top loading and unloading
AAR-112	A pressurized tank car that has additional safety features than what is required on DOT-111 class non-pressurized tank cars.

Type	Meaning
DOT-114	Insulated or non-insulated, carbon or alloy steel with a manway nozzle and optional noncircular cross-section
DOT-120	Insulated carbon steel or aluminum alloy with a manway nozzle
Cryogenic Liquid Designations	
DOT-113	Vacuum insulated with a high alloy or nickel inner container (tank) and carbon steel outer shell (tank, not jacket)
AAR-204	Vacuum insulated with an inner alloy steel container (tank) and carbon steel outer shell (tank, not jacket); similar to DOT-113

In North American freight railroads, the fleet of tank cars is ever changing. New cars are continuously built and put into use while older cars are retired and removed from service. Additionally, many tank cars are altered or stored temporarily until they are needed. Details on the current tank car, new builds, and retrofit details can be found on the Railway Supply Institute webpage.[1] Figure 2 shows the amount of the railroad tank cars in North America that transported Class 3 flammable liquid in 2020. A flammable liquid (Class 3) means a liquid having a flash point of not more than 60 °C (140 °F), or any material in a liquid phase with a flash point at or above 37.8 °C (100 °F) that is intentionally heated and offered for transportation or transported at or above its flash point in a bulk packaging.[2] These include liquids such as refined petroleum products, crude oil, and ethanol.

In 2020, 111,177 railroad tank cars transported Class 3 flammable liquids, a decline of 1.3 percent compared to 2019 [6]. In Figure 2, "All Other Rail Tank Cars" include DOT-105, DOT-112, DOT-114, and DOT-120 rail tank cars, are pressurized and already exceed the DOT-117 specification, and DOT-115 and DOT-211 rail tank cars, which do not typically carry crude oil or ethanol, but may carry other flammable liquids. Similarly, "Other Flammable Liquids" includes all flammable liquids that are not crude oil or ethanol. The tank car fleet has changed in recent years in terms of its compositions and the types of flammable liquids often transported. This change is mainly attributed to the growth and adoption of the DOT-117 and 117R tank cars. For example, in 2017, only 58 non-jacketed DOT-111 cars carried any shipments of crude oil. This number was close to zero in 2018, meeting the Fixing America's Surface Transportation Act (FAST Act) legislation phase-out deadline of January 1, 2018. Only 27 non-jacketed CPC-1232 cars carrying petroleum crude oil were used before April 1, 2020. Finally, due to some rail tank cars carrying different fluids in a year, these are classified for use for multiple service liquids, and they do not have one phase-out date because there are multiple phase-out dates.

[1] Railway Supply Institute webpage.

[2] Electronic Code of Federal Regulations. 49 CFR § 173.120–*Class 3 - Definitions*. National Archives and Records Administration.

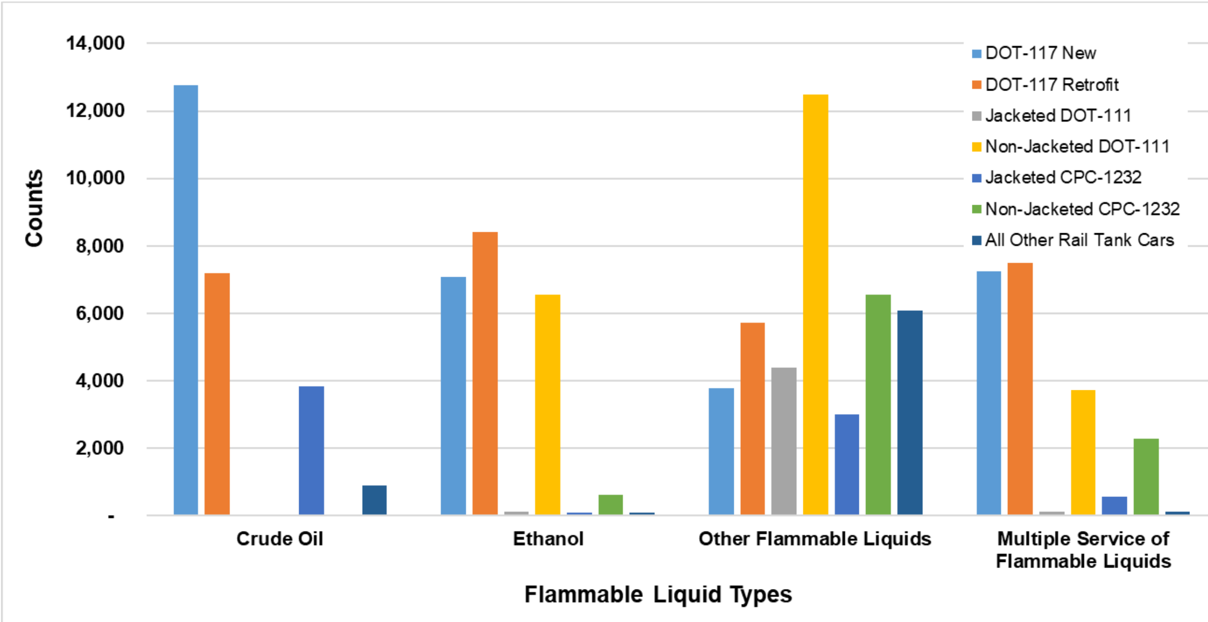

Figure 2. Distribution of railroad tank car types transporting flammable liquid in 2020
SOURCE: DOT Bureau of Transportation Statistics. Special analysis based on data provided by the AAR: UMLER® and TRAIN II® 2013–2020, as of June 2021

3. Corrosion Overview and Monitoring Techniques

Corrosion occurs when metals naturally degrade due to a chemical reaction. It progresses continually and occurs in areas not easily accessible to inspection, cleaning, or periodic re-coating. Over time, if not mitigated, corrosion will destroy the substrate. Corrosion can result in both material strength and structure loss [7, 8]. Corrosion occurs when the base metal is exposed to catalysts such as air, water, and other corrosive elements/materials. Many factors influence the rate of corrosion. The corrosive media is the most important factor, but other factors include temperature, pressure, diffusion of reactants to and from the metal surface, conductivity, pH values, chemical concentration, type of ions (chloride and Sulphur), electrochemical potential, type of flow of fluid (laminar, transitional, and turbulent) relative to the metal surface, material types, and the effect of condensation [7, 9–11]. Formation of rust is the most common example of electrochemical corrosion, and it consists of the anodic dissolution of metals and the cathodic reduction of oxidants present in the aqueous solution. Similarly, the presence of an oxidant such as hydrogen sulfide (H_2S) and carbon dioxide (CO_2) can cause severe corrosion in the pipeline and tanks that carry commodities that contain these compounds. Standard methods to guard against corrosion progression include sealing, coating, or painting substrate surfaces. Cathodic protection and the presence or absence of inhibitors or accelerators, such as the degree of oxidizing power of the catalyst or exposure to air, pH stabilization influence the corrosion rate. Such prevention and mitigation methods can slow down the rate of progress but, ultimately, seldom prevent corrosion.

3.1 Types of Corrosion

The various forms and combinations of corrosion must be understood to both determine the importance of each and find the most appropriate technologies for the detection/characterization of corrosion and appropriate mitigation strategies. Tank cars can suffer from corrosion in several forms, and inspectors must identify the damage it causes, visually or with the use of NDE methods. Some of the different types of corrosion that affect the tank car shell include uniform corrosion, sweet corrosion (CO_2 corrosion), sour corrosion (H_2S corrosion), localized corrosion, stress corrosion, and intergranular corrosion. These types of corrosion can be defined as follows:

- Uniform corrosion is metal being attacked evenly over its entire surface or over a large part of its surface that is wetted within the corrosive environment. Rusting is the most common form of uniform corrosion, with the level of degradation being uniform on all sections of the tank car. It appears as irregular roughening of the surface that can cause scale to form. This type of corrosion can be mitigated by removing the surface corrosion and coating the surface to protect it from the environmental elements.
- Sweet corrosion or corrosion resulting from CO_2 is generally induced when CO_2 gets dissolved in an aqueous phase. This typically occurs in the tank carrying petroleum products containing CO_2 that, when dissolved in water, becomes corrosive and accelerates due to formation of iron carbide [9, 12, 13]. The major forms of CO_2 corrosion include pitting and mesa (i.e., exposure to conditions of wet carbon dioxide at elevated temperatures).
- Sour corrosion is a corrosion resulting from H_2S and moisture. H_2S levels above 0.05 psi of partial pressure are considered sour by the National Association of Corrosion

Engineers (NACE). H_2S is a weak acid that is not corrosive when dissolved in water. However, it releases hydrogen in water that is corrosive and can lead to hydrogen embrittlement [14–17]. Also, sour corrosion mechanisms reportedly have different characteristics when it comes to surface appearances and morphology [18]. The major forms of sour corrosion are uniform/general and localized, pitting, crevice corrosions, and stepwise cracking.

- Localized corrosion, including pitting, crevice, and filiform corrosion, can occur at a specific area of the tank surfaces.
  - Pitting is characterized by holes with a circular shape and a hemispherical bottom produced in the material in a non-uniform fashion at a specific location. Pitting is difficult to detect because of its size and shape. Pits can be both narrow and deep to shallow and wide and can weaken the material and cause it to fail if too much material is lost.
  - Crevice corrosion typically occurs in the areas of the mechanical joints, such as coupled pipes or threaded connections, typically in an area in the form of a crevice or narrow clearances with debris deposit. It forms on the surface of a metal exposed to an aqueous environment. Accelerated corrosion can be expected to occur within the crevice or debris deposit. It is triggered by local differences in environment composition (i.e., oxygen concentration). The appearance of crevice corrosion is scale and pitting.
  - Filiform corrosion builds up under coated/painted surfaces. The mechanism for corrosion allows water and oxygen to migrate. This type of corrosion has a tendency of taking place in conditions with a high level of humidity. Filiform corrosion occurs in places with conditions slightly above room temperature and a humidity level of 75 percent [19]. The coating will bulge because of the corrosion.
- Galvanic corrosion is an electrochemical process where one metal corrodes preferentially to another when both metals are in electrical contact. Metals and metal alloys all possess different electrode potentials. The electrolyte acts as a conduit for ion migration, moving metal ions from the anode to the cathode. As a result, the anode metal corrodes more quickly than it would otherwise, while the cathode metal corrodes more slowly and, in some cases, may not corrode at all.
- Stress corrosion is the cracking induced from the combined influence of tensile stress and a corrosive environment. This type of corrosion occurs by the combined and simultaneous action of corrosion and a static tensile stress. Corrosion fatigue is caused by cyclic stressing in mildly corrosive environments.
- Intergranular corrosion initiates at the microscopic level within the material. All solid metals are crystalline in nature. Therefore, all metallic structures consist of a multitude of tiny crystals called grains. When corrosion occurs preferentially along the boundaries of these grains, the metal is said to experience intergranular corrosion.

Corrosion associated with railroad tank cars is somewhat different than what is encountered with stationary tank storage and pipelines and can be influenced by many factors, including the external environment, commodities, and loading stresses. Repetitive loading and unloading can create microscopic tank shell cracks that propagate little by little with each subsequent cycle, and these microscopic breaks in the metal that create initiation points for corrosion to form. Tank cars carrying corrosive products often require special linings or coatings to protect the inner tank shell, but these coatings are also subject to aging. Even after unloading, the residual product can elevate corrosive factors such as aeration, liquid, and vapor phases in prolonged contact, and the presence of moisture [20]. Figure 3 shows an example of uniform corrosion and pitting on the interior of a tank car.

Figure 3. Uniform corrosion and pitting on interior of tank car

In addition, corrosion occurs on the outer diameter of the tank shell on tank cars with an outer protective jacket and insulation/thermal protection. Insulation traps moisture against the steel walls allowing it to react to the metal over a long period. Because this occurs under the jacket and the insulation, corrosion can form without being detected. This is often referred to as corrosion under insulation (CUI). Prolonged corrosion can develop during service, leading to a structure breakdown that can cause leakage of the contents to the environment and physical injury. Figure 4 shows an example of corrosion and pitting on the outer diameter of a tank shell under insulation.

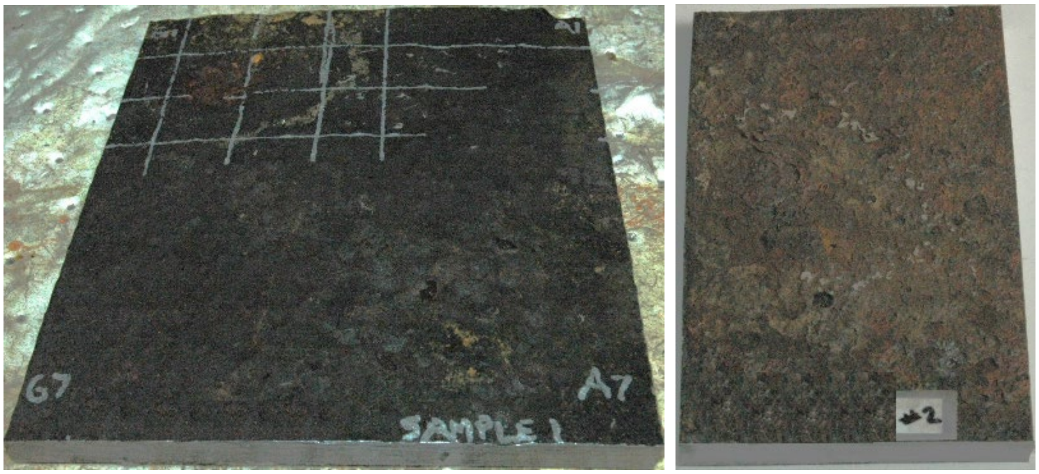

Figure 4. Corrosion and pitting on the outer diameter of tank shell with insulation

3.2 Effects of Corrosion

Corrosion is a highly complex technical issue, and its causes and effects are not completely understood. Corrosive chemicals attack metal surfaces in different ways, as exemplified by an issue that the tank car industry is dealing with on tank cars that deliver crude oil. The tank cars designed to carry crude oil are not performing equally in service. Crude oil is classified as sweet or sour. Sweet crude oil contains less than 0.5 percent sulfur while sour crude oil contains levels greater than 0.5 percent sulfur. The tank car industry is seeing more bath-ring-type corrosion on the inner diameter (ID) running the length of the cars in sour crude oil service than on the cars in sweet crude oil service. While the cause seems obvious, the method of mitigation is not. It is not feasible in the context of the railroad operating environment to have specific cars for the same bulk product. The following example emphasizes the importance of detecting and mitigating corrosion in the existing tank car fleet.

3.3 Corrosion Prevention, Mitigation, and Prediction

Corrosion is the main challenge affecting the structural integrity of many components including the oil and gas pipelines and tanks. The appearance of corrosion, in and of itself, is not a failure of the material, but if left unchecked, corrosion can and will create points in the material where failure can occur. The best response to corrosion is to mitigate the corrosion by removing it from the material. If there is a substantial amount of material loss, the material may need to be built back up by welding or other means, if allowed, and then treating the corroded area by applying sealants or protective coverings to prevent corrosion in the future.

Effective corrosion prevention techniques can help extend the life of a tank car. Several methods are used to inhibit the rate of corrosion or prevent metal from corroding in the first place. These are typically generalized into three groups: metal treatment (selection of material), treatment of environment (removal of H_2O, H_2S, CO_2, O_2, and salts) and treatment of boundary metal environment (cathodic protection, coatings, and injection of inhibitors) [7]. A proper selection of materials includes metals, alloys, polymers, and composites appropriate for commodities to transport. However, there is no ideal material that 1) can be used under all conditions and 2) has resistance to all mediums [10].

Painting over the exposed metal surface is a cost-effective way to protect the metal. Paint coatings act as a barrier to prevent the transfer of electrochemical charge from the corrosive solution to the metal underneath. When corrosion is found, it can be removed through mechanical means like grinding or abrasive blasting or using chemicals to dissolve light corrosion. Once the corrosion has been removed, painting the area will protect the surface from further corrosion. Paint is often used as a first line of defense against corrosion on the exterior of tank cars. Interior coatings other than paint are used to protect the inside of the tank.

Using a metal to plate the steel can add a protective cladding to the base metal. An additional metal coating can safeguard the base metal by sacrificing itself while shielding against a corrosive environment. The two main techniques for achieving a sacrificial coating are cathodic and anodic protection. Galvanizing is cathodic protection coating an alloy steel with zinc. Zinc is a more active metal than steel, therefore, when it starts to corrode, it oxidizes and inhibits the corrosion of the steel. Anodic protection involves coating steel with a less active metal like tin. Tin will not corrode, thereby protecting the steel underneath, so long as there is a layer of tin covering it.

Similarly, a metal surface can be protected by covering it with a material that insulates the metal from the environment that would normally cause it to corrode. This insulation consists of thicker coatings like plastics, rubbers, or chemical resistant epoxies that create layers between the corrosive solution and the metal. The thicker layer of protection can provide a longer corrosion resistant life and aid in resisting abrasive wear and impacts.

Finally, methods used to alter chemical composition of environment encompass methods that 1) eliminate H_2O, H_2S and CO_2 from crude oil, 2) stabilize the pH, and 3) inject corrosion inhibitors and biocides [21, 22].

According to 49 CFR § 180.509, each tank car owner must ensure qualification of the tank car safety systems [2]. The specific excerpt from the regulation regarding internal coatings reads:

> (i) *Internal coating and lining inspection and test.*
>
> > (1) At a minimum, the owner of an internal coating or lining applied to protect a tank used to transport a material that is corrosive or reactive to the tank must ensure an inspection adequate enough to detect defects or other conditions that could reduce the design level of reliability and safety of the tank is performed.

Just as there are many forms and combinations of corrosion, there are many different means to characterize the rate of corrosion including the weight loss, electrochemical, and accelerated testing methods, the use of software applications, and NDE methods [7, 23]. No single means of detection is either ideal or even suitable for all forms of corrosion. Over the past 30 years, great progress has been made in the modeling and understanding of crack growth. At least partially due to the many forms and combinations of corrosion, each with different outcomes, similar progress has not been made in the modeling and prediction of corrosion. Prediction of corrosion damage now relies heavily on periodic inspection to find and measure the effects of the many forms of corrosion.

3.4 Tank Car Shell Thickness Measurement

CFR § 180.509(f)(2) specifies thickness tests for the corrosion detection and monitoring for the tank cars [2]. The tank car owner must ensure each tank car facility measures the thickness of the tank car shell, heads, sumps, protective housing (i.e., domes), and nozzles on each tank car by using a device capable of accurately measuring the thickness to within ±0.05 mm (±0.002 inches). The tank car owner must ensure that each tank car has a thickness test measurement as specified in CFR § 180.509(f)(2):

i. At the time of an internal coating or lining application or replacement, or

ii. At least once every ten (10) years for a tank that does not have an internal coating or lining, or

iii. At least once every five (5) years for a tank that does not have an internal coating or lining when:

   A. The tank is used to transport a material that is corrosive or reactive to the tank or service equipment as defined in part § 180.503, and

   B. The remaining shell and head thickness is tested and determined to be at or below line C as shown in Figure 5 (of this report).

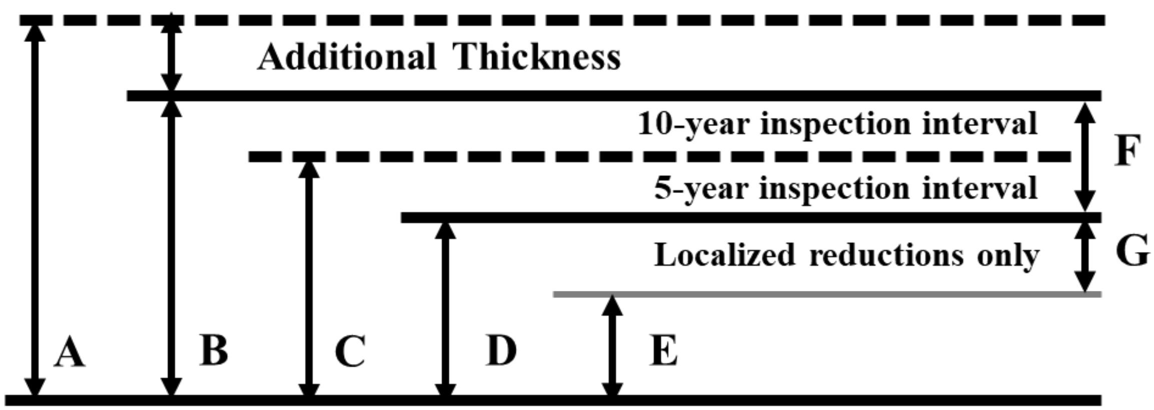

Figure 5. Tank and shell thickness qualification frequencies

The letter designations in Figure 5 are defined as follows from § 180.509(f)(2):

A. As-built tank shell or head thickness with additional thickness.

B. Required minimum tank shell or head thickness after forming per part 179.

C. Inspection frequency adjustment point (design minimum shell or head thickness, minus 1/2 of the value shown in Table 2).

D. Condemning limit for general corrosion (required minimum shell or head thickness, minus the value shown in Table 2).

E. Condemning limit for localized corrosion (required minimum shell or head thickness, minus the value shown in Table 2, minus 1.58 mm (1/16 inch)). Refer to the note for diameter limitations and minimum separation distances at the end of next paragraph.

F. Allowable shell or head thickness reduction (value shown in Table 2).

G. Additional thickness reduction for localized areas in value shown in Table 2 of this section.

Table 2. Allowable shell thickness reductions (paragraph g, § 180.509)

Marked tank test pressure	Top shell and tank head	Bottom shell
60 psig <200 psig	3.17 mm 1/8 inch	1.58 mm 1/16 inch
≥200 psig	0.79 mm 1/32 inch	0.79 mm 1/32 inch

Note that a tank car owner may add an extra 1.58 mm (1/16 inches) to the values in the table for local reductions. Local reductions are those 1) that do not exceed 20.32 linear centimeters (8 linear inches) measured at the longest diameter and 2) that are separated from the other local reductions by at least 40.64 cm (16 inches).

While the CFR requires a device capable of accurately measuring the thickness to within ±0.05 mm (±0.002 inches), today, this can only be achieved using a thickness dial indicator/gauge or using ultrasonic thickness (UTT) gauge NDE equipment. However, these UTT measurement techniques are approaches that would require conducting measurements in several locations. The big issue with this approach is that the integrity of the entire tank would need to be assumed based on the limited area where measurements are taken. Real-time area scanning NDE methods for corrosion monitoring and remaining shell thickness measurements would provide incredible benefits to the industry. Also, it would allow engineers to digitally record the data and conduct more analysis later.

3.5 Corrosion Monitoring NDE Technologies

Current best practices for monitoring corrosion include visual checks of the material for abrasion, corrosion, pitting, cracks, and dents. Corrosion can be found through visual inspections of the external surface, accessible piping, valve fittings, and gaskets. NDE technologies play an important role in the continued safe operation of physical assets. Depending upon the nature of the component, the type and location of corrosion, and the access to the location, several NDE methods detected and characterized corrosion in different applications. The most common NDE methods for corrosion monitoring and detection include visual (i.e., regular, remote, aided, and enhanced), liquid penetrant, conventional ultrasonics, UTT measurements, eddy current, magnetic flux leakage (MFL), and radiographic testing (RT). Each different corrosion NDE detection technology entails different training requirements. For example, eddy current and ultrasonic sensors produce displays that require a high degree of sophistication to properly interpret.

Improved processing of newer techniques, such as pulsed eddy current and advanced phased array UT, provide c-scan images that are much more intuitive but still require expert interpretation, especially in determining when a particular threshold has been exceeded and repair is required. The range of technologies also expands the knowledge required to interpret the results. Thus, for a technician to be considered fully qualified in all areas necessary to perform a complete corrosion inspection, many more skills are required now than before. As in so many other areas, the area of corrosion detection is limited by a probability of detection and by the characterization and accuracy of the results. Much of the corrosion inspection work is repetitive, tedious, and sometimes done in awkward locations and under adverse environmental conditions (e.g., darkness, direct sunlight, heat, and cold), the corrosion inspection problems extend well beyond just the technology of the sensing device and the processing of the information. Both the sensing device and the information processing must include an array of human factors that will limit the overall effectiveness of the inspection process.

Some of the advanced NDE methods investigated by researchers to improve corrosion detection and measurements in different applications include optical surface topography [24, 25], optical metrology methods [26], phased array ultrasonics [27], electromagnetics [28–32], EMATs [33–35], MFL [36, 37], infrared thermography (IRT) [38, 39], microwave and millimeter waves [40, 41], terahertz imaging [42], and X-ray backscatter radiography [43, 44]. In addition to these, pipeline inspection gauges (pigs) are also often used for the in-line inspection (ILI) or in-line monitoring (ILM) of pipelines in which pigs are often retrofitted with NDE instruments such as UT, EMATS, or MFL sensors [45–47]. Pigging involves inserting pigs into pipelines at valve or pump stations where the valves and pipes have special configurations that allow pigs to be loaded into launchers. Product flow drives the pig through the line until it reaches the pig receiver, at which point it is retracted from the line.

Regardless of the size of the pipeline, pipe pigging can be performed without interrupting the flow of material. ILI tools allow the identification of critical zones with external corrosion or mechanical damage. Advancement in computing power, micro-electronics and optics, imaging, signal processing, and software have all been adapted to a next generation of field deployable NDE equipment capable of enhanced inspection productivity at refineries, chemical plants, pipelines, and offshore production sites. However, all the NDE methods discussed have their own advantages and limitations, and they are often used interchangeably in the field to aid the limitations of other methods and exploit the benefits for direct assessment to identify appropriate remediation.

Above all, one of the most challenging situations for corrosion inspection is CUI, which is one of the major challenges that is commonly faced by several industries including aerospace, transportation, oil/gas, and petrochemical [27, 48, 49]. This challenge will also hold true for the tank car industries that has jacketed tanks in service. Due to the trapped moisture between the jacket and tank shell, a corrosive environment that will accelerate the corrosion in the tank walls can be formed between the insulation and the metal wall. It is reported that between 40 percent and 60 percent of pipeline repairing costs in the oil and gas industry are related to CUI [48]. To develop a rigorous inspection and monitoring plan for CUI, a structured and systematic approach must be considered by looking into more invasive approaches. The inspection plan should consider operating temperature, commodities information, type and age/condition of coating, and insulation material. CUI damage may continue to occur even if external insulation appears to be in good condition. CUI inspection may require removal of some or all insulation. If external coverings are in good condition and there is no reason to suspect damage behind them, it may not be necessary to remove them for inspection of the tank. CUI is normally inspected using digital radiography, ultrasonic spot thickness reading, pulsed eddy current, and insulation removal approaches. Several advanced NDE methods, including infrared thermography and wide range of array eddy current testing, are used for CUI inspection.

4. Surveyed Tank Cars

The research team surveyed several examples of tank cars with corrosion and inspected at the Transportation Technology Center (TTC) near Pueblo, CO. These tank cars represented those that were retired or donated for other testing purposes. Some of the tank cars surveyed had a layer of steel surrounding the tank shell and are known as jacketed tank cars. These jackets are an essential safety feature of a rail tank car, and they protect the inner tank to prevent or limit massive leaks, explosions, and other disasters that occur when tanks carrying HazMat derail. The jacket holds an insulation layer between the jacket and the tank shell. The outer jacket can corrode from spilled chemicals on the outside. External corrosion also occurs from water on the damaged part of the jacket, missing paint, cracks, or breaks from damage done to the car. When water seeps between the jacket and the tank, it can have a negative impact on the metal of the tank car and corrode the outside diameter of the inner tank shell. In cases when tank cars have insulation, the insulation can hold the water next to the outer tank shell walls giving it more time to act on the metal, thereby accelerating the corrosion process. Figure 6 shows a corroded DOT-105A tank car and a pressurized and jacketed tank car. Cracks, dings, or poor welds left this tank car susceptible to moisture getting between the tank car's outer protective shell and the inner tank. Insulation between the shell and the tank car trapped moisture against the steel. Prolonged moisture exposure caused rusting from the backside of the outer shell.

Figure 6. DOT-105A car with rust on outer jacket

Figure 7 shows a DOT-112T tank car with an outer jacket. Despite being coated with insulation around the outside, this car suffered cracks in the insulation membrane, allowing water to seep beneath the insulation and get trapped between the insulation and the steel. Visual inspection cannot directly observe corrosion under the jacket, although indications of the corrosion exist as rust stains on the outer jacket. Similarly, ultrasonic, magnetic particle, and eddy current inspections will not work on tank cars with outside-car insulation. Access to the base material is required for these technologies to be effective. A radiography inspection could identify loss of material, and thermography could identify how much of the area has been affected by water creep, but thermography is not currently an approved inspection method.

Figure 7. DOT-112T tank car with a crack in the external jacket

Figure 8. DOT-105J tank car with corrosion from inside the jacket

Figure 8 shows photos of a DOT-105J tank car, a pressurized tank car with a jacket. This car shows evidence of severe corrosion on the outer jacket. Water entering a break in the jacket traveled down the side of the tank car and settled in the belly of the car. Extended contact with water caused a complete perforation of the steel jacket near its attachment point at the sill.

Figure 9. DOT-111A tank car with corrosion

Figure 9 shows photos of a DOT-111A tank car, a non-pressurized tank car with no jacket. This tank car shows bands of uniform corrosion along the underside of the tank. These rusty areas are in line with the wheels of the car. The wheels flinging debris and water up onto the bottom of the tank creates spots for corrosion to take hold. At the stage of corrosion shown here, mitigation is possible. Removing the corrosion and painting the affected area to seal the steel from the environment would be effective methods of mitigation.

In addition, tank car industry professionals participated in a brief survey to understand the common challenges presented by corrosion. Based on these discussions, it was discovered that the area of corrosion inside the tank car depends on the material it transports. Figure 10 depicts the areas around the inside tank perimeter where corrosion is common for several commodities.

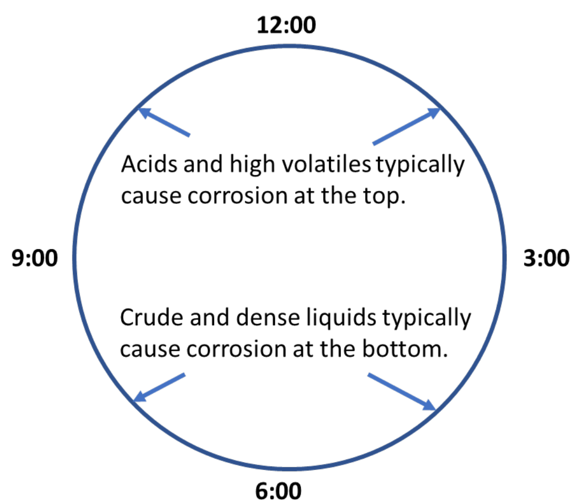

Figure 10. Clock face diagram depicting where corrosion is likely for various commodities

Acids and chlorine typically cause corrosion in a band around the top of the tank car at the 10:00 and 2:00 o'clock positions. Crude oil, with heavy sediments, typically causes corrosion in a band along the bottom at the 5:00 and 7:00 o'clock positions. Corrosion can also occur in areas such as the nozzle body or near the valves. Sodium bisulfite and ammonium nitrate are solid catalysts for corrosion and tend to attack unprotected metal anywhere contact occurs. The interior of the tank car is cleaned, and then inspected by specially trained inspectors who enter the tank. The inspection area is the bottom third of the tank because this is the region that has the most significant potential for corrosion. Lined tanks must be removed before inspection because the liner can hide defects.

Corrosion on the jacket is considered a cosmetic condition. Where holes form due to corrosion, the fix can be to weld a plate over the jacket covering the open area. When the inner tank shows corrosion, whether on the exterior or interior of the tank, the corroded area will need to be mitigated through additional work. When the steel plates show pitting, the area will need to be cleaned, ground, and welded to build the metal up to its original thickness before it is ground flush with the surrounding.

Bolsters, cradles, and head blocks are usually hidden beneath the jacket. In these cases, parts of the jacket must be removed to allow visual, penetrant, and ultrasonic inspection. Painted areas will need to have the paint removed before any inspection. Once the inspection is complete and any repairs are made, the part is painted, and a plate is welded over the opening.

5. Corrosion Test Panels Development

To test the capabilities of different NDE methods for corrosion monitoring, detection, and characterization, proper test coupons should be produced. For optimal results, it is recommended that test coupons are prepared from the actual tank car material to eliminate material variation (sensitive to NDE methods) during NDE applications.

5.1 Tank Car Corrosion Test Panel

The tank cars surveyed at the TTC and those that had some amount of corrosion present were selected for developing the first round of test panels. The corrosion on these tank cars (inner shell and outer jackets) was mostly light except on a few cars that had a major amount of corrosion. The corrosion on these tank cars was present in various locations. Out of these tank cars, a DOT-105J tank car (as shown in Figure 8) was selected for making the first round of test panels. A total of seven test panels were cut from different locations on the DOT-105J tank car had good amount of corrosion present. These panels are shown in Figure 11, and Table 3 provides the description of these test panels. After the test panel locations were selected and cut out from the tank car, 1-inches square grids were marked on the surface of the samples to map the wall thickness using UTT measurements. Figure 12 shows examples of the test panels with grid markings. A brief description of these test panels is also provided below.

Figure 11. Locations on the tank car for test panel development

The thickness of the DOT-105 tank shell varies based on DOT specifications and the bursting/ test pressures. Although for DOT-105 cars, the minimum plate thickness specified is 5/8-inch, 9/16-inch, and 11/16-inch (49 CFR § 179.100 [2]), the original plate thickness of the tank car shells was recorded as 0.775-inches. Similarly, the steel jacket thickness is usually around 11 gauge (0.125-inches), but the thickness measured in some plates was considerably higher. It is assumed that this discrepancy was due to the replacement of materials with different size gauge materials during jacket repairs. Nevertheless, these plates aim to access the capability of NDE systems or methods to accurately detect and characterize corrosion and estimate the plate thickness based on what is currently known.

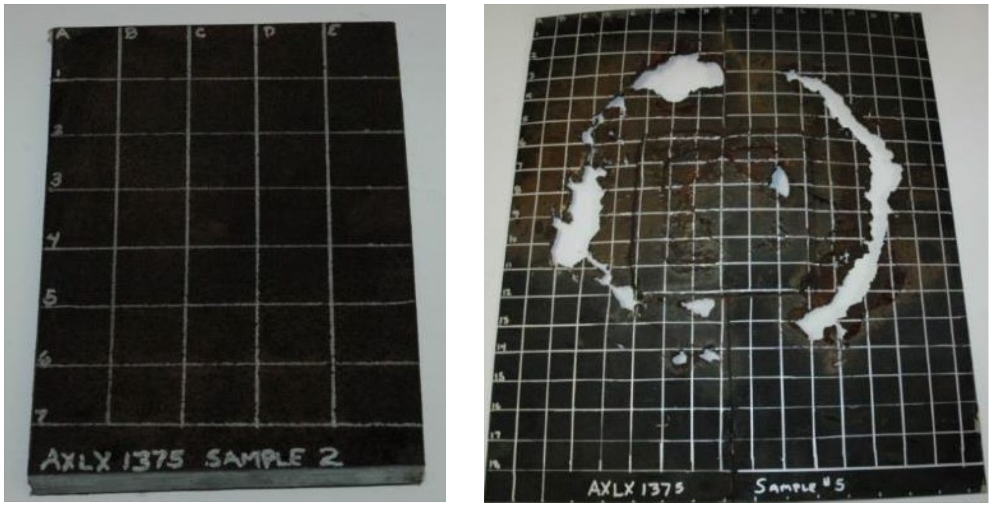

(a) (b)

Figure 12. 1-inch x 1-inch grid markings on the test panels: (a) tank shell; (b) tank jacket

Table 3. Description of test panels made from DOT-105J tank car

Test Panel #	Sample Description	Location in Tank Car	Sample Dimensions [inch]	Original Nominal Thickness [inch]
1	Tank Shell	Under the tank (belly)	6.750 x 7.625	0.775
2	Tank Shell	Under the tank (belly)	5.250 x 7.750	0.775
3	Tank Jacket	Under the tank (belly)	6.875 x 11.750	0.125
4	Tank Jacket	Under the ladder on the left side	11.875 x 12.000	0.125
5	Tank Jacket	Top center of the car	16.750 x 19.250	0.125
6	Tank Jacket	Top right of the car	19.000 x 25.000	0.125
7	Tank Jacket	Top of the car	19.750 x 35.000	0.125

Test Panel 1

Figure 13 shows test panel 1. This panel was made from the inside shell of the tank car and exhibits a significant amount of corrosion on its outside surface (OD) and wall loss on its inside surface.

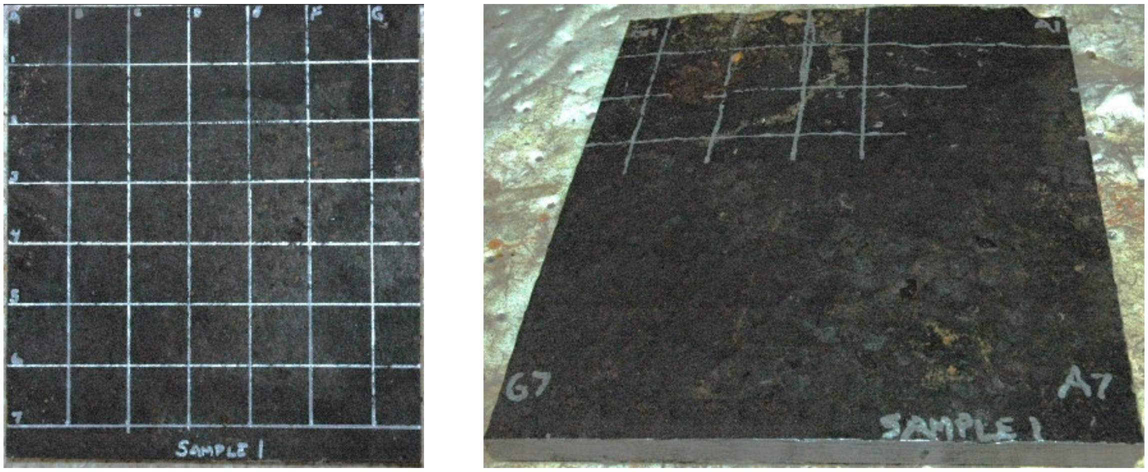

(a) (b)

Figure 13. DOT-105J test panel 1: (a) ID; (b) OD

Test Panel 2

Figure 14 shows test panel 2. This panel was also made from the inside shell of the tank car and exhibits a moderate amount of corrosion on its outside surface (OD) and wall loss on its inside surface.

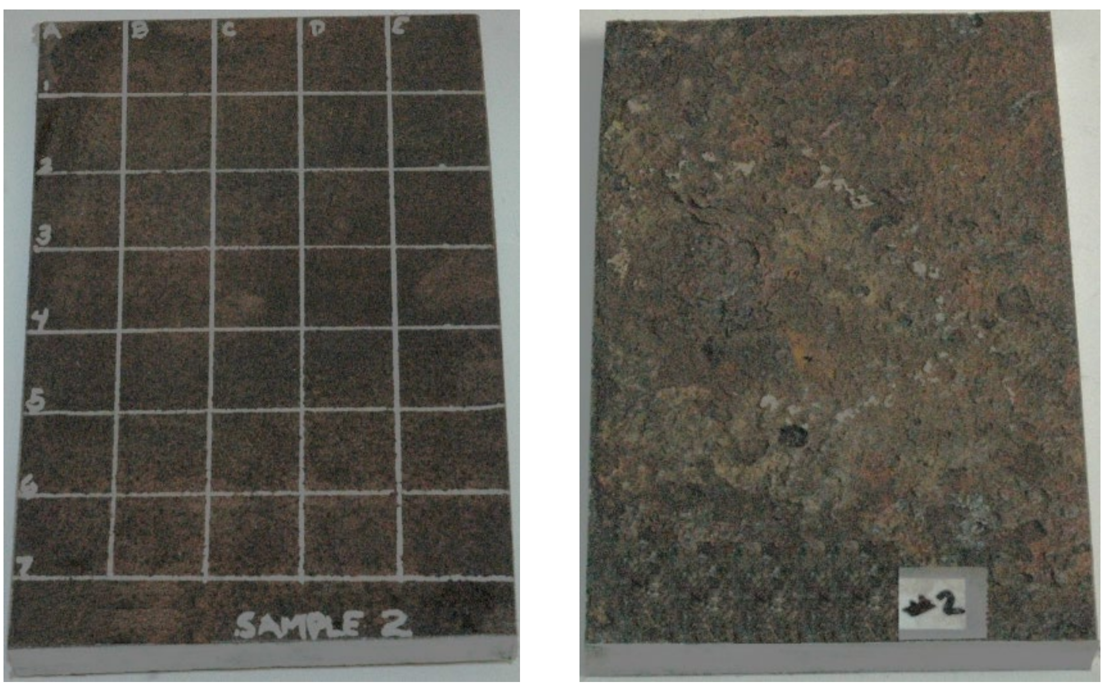

(a) (b)

Figure 14. DOT-105J test panel 2: (a) ID; (b) OD

Test Panel 3

Figure 15 shows the test panel 3. This panel was also made from the tank jacket material and exhibited corrosion on its inside surface (ID).

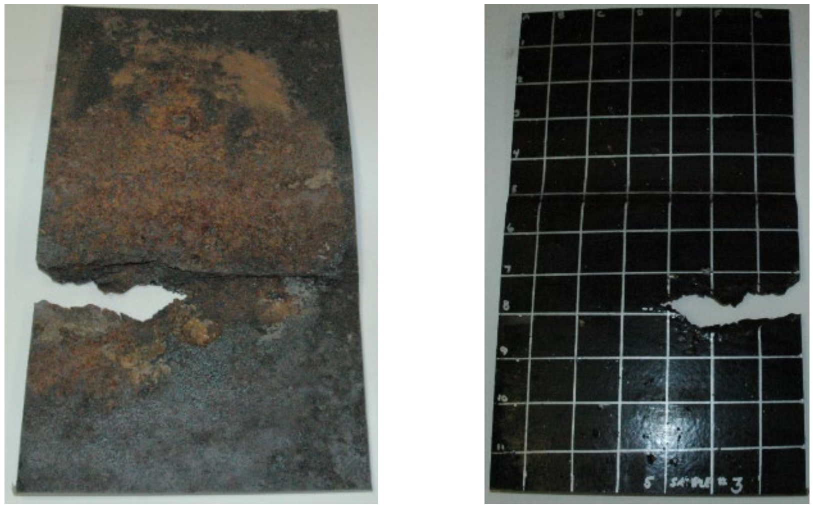

(a) (b)

Figure 15. DOT-105J test panel 3: (a) ID; (b) OD

Test Panel 4

Figure 16 shows the test panel 4. This panel was also taken from the tank jacket material and exhibited corrosion on its inside surface (ID).

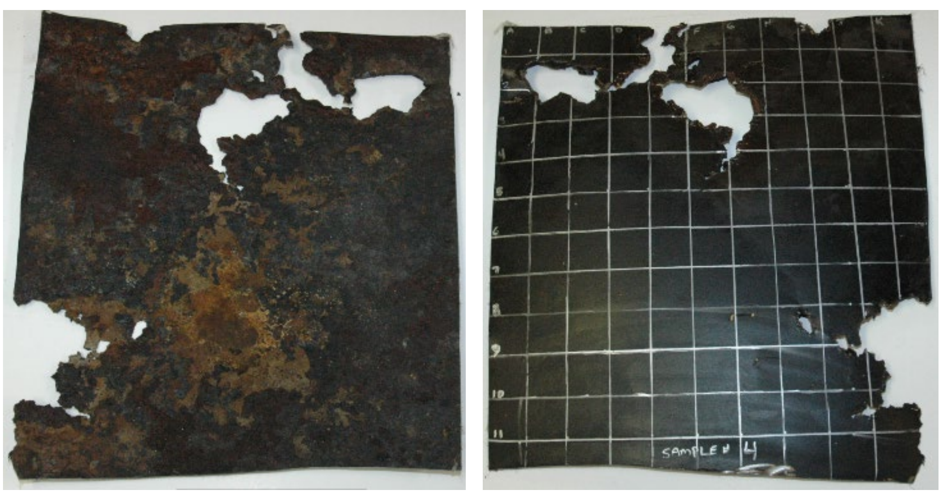

(a) (b)

Figure 16. DOT-105J test panel 4: (a) ID; (b) OD

Test Panel 5

Figure 17 shows test panel 5. This panel was also taken from the tank jacket material and exhibited corrosion on its inside surface (ID).

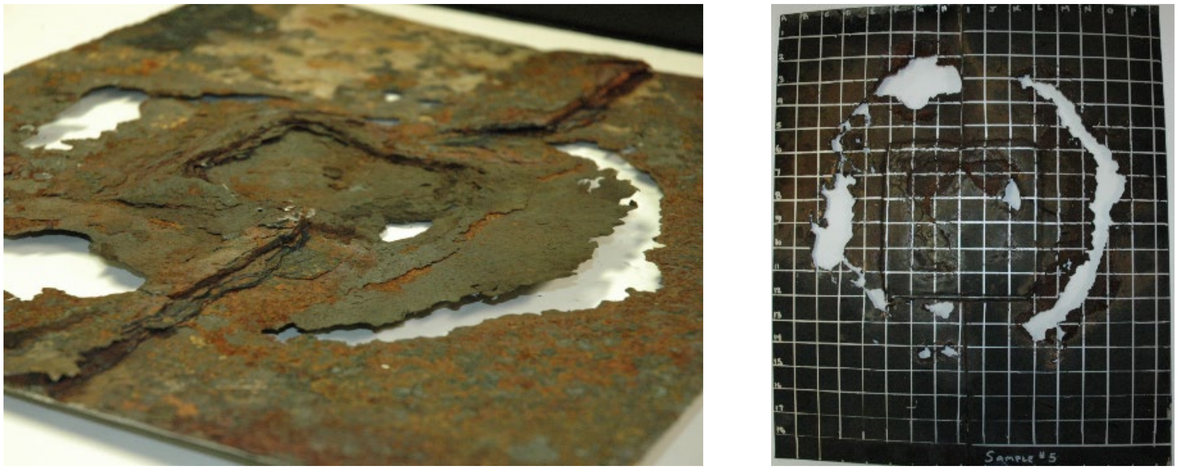

(a) (b)

Figure 17. DOT-105J test panel 5: (a) ID; (b) OD

Test Panel 6

Figure 18 shows test panel 6. This panel was also cut from the tank jacket material and exhibited corrosion on its inside surface (ID).

Figure 18. DOT-105J test panel 6, OD

Test Panel 7

Figure 19 shows test panel 7. This panel was also made from the tank jacket material and exhibited corrosion on its inside surface (ID).

(a)

(b)

Figure 19. DOT-105J test panel 7: (a) ID; (b) OD

5.2 Tank Car Corrosion Reflector Plates

The second round of test samples consisted of three different tank car reflector plates cut from one of the DOT-117 tank car shells. The DOT-117 (also referred to as TC-117 in Canada) is a non-pressurized tank car for transporting Class 3 flammable liquids across North American railroads. The design of the DOT-117 tank car was an upgrade to the specifications of the then-common DOT-111 and CPC-1232 tank cars. Executed on December 2015, the FAST Act mandated the phasing out of tank cars built to lower safety standards and prohibiting the transportation of Class 3 flammables with DOT-111 tanks by 2029. The CFR and AAR specifications require that the tank shells be constructed out of 0.5625-inch-thick normalized TC-128 Grade B steel with 11-gauge (0.125-inches) sheet metal jackets, 0.5-inch-thick head shields on the ends of the tanks, and improved valves over previous designs.

Different sized (diameter and depth) holes were drilled on the surface of these plates. Tank car reflector plate 001 had flat bottom holes (FBHs) ranging from 0.06-inch to 1-inch in diameter drilled on its surface (Figure 20). Similarly, tank car reflector plate 002 had FBHs ranging from 0.06-inch to 1-inch in diameter drilled on its surface (Figure 21). Tank car reflector plate 003 had round bottom holes ranging from 0.063-inch to 0.5-inch in diameter drilled on its surface (Figure 22). The goal of these plates is to allow access to the capability of NDE systems or methods that can accurately detect and size these holes with and without insulation.

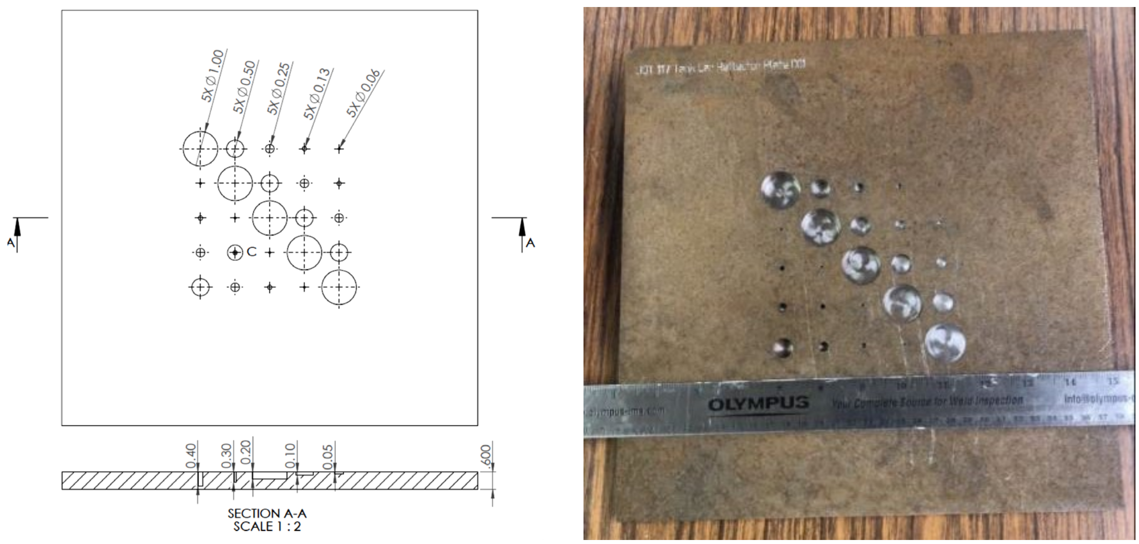

(a) (b)

Figure 20. DOT-117 tank car corrosion reflector plate 001: (a) engineering drawing; (b) as-built part (dimension in inches)

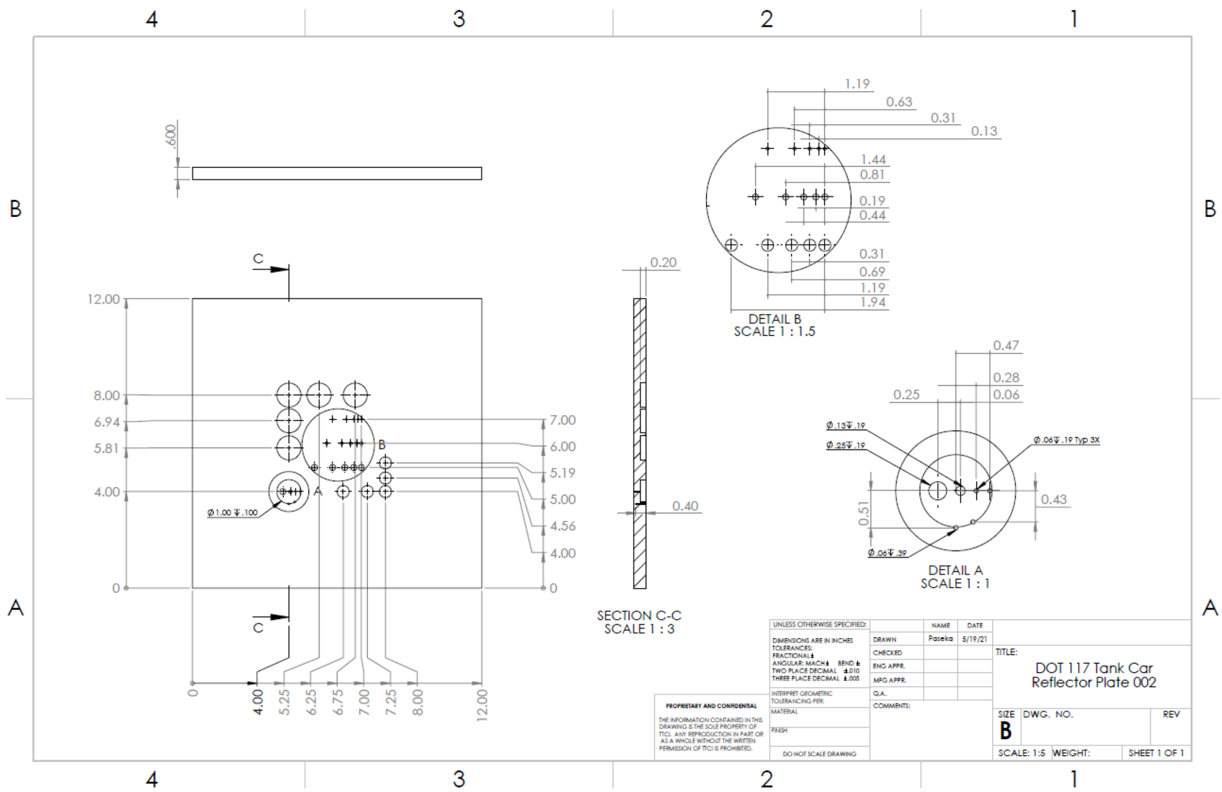

(a)

(b)

Figure 21. DOT-117 tank car corrosion reflector plate 002: (a) engineering drawing; (b) as-built part (dimension in inches)

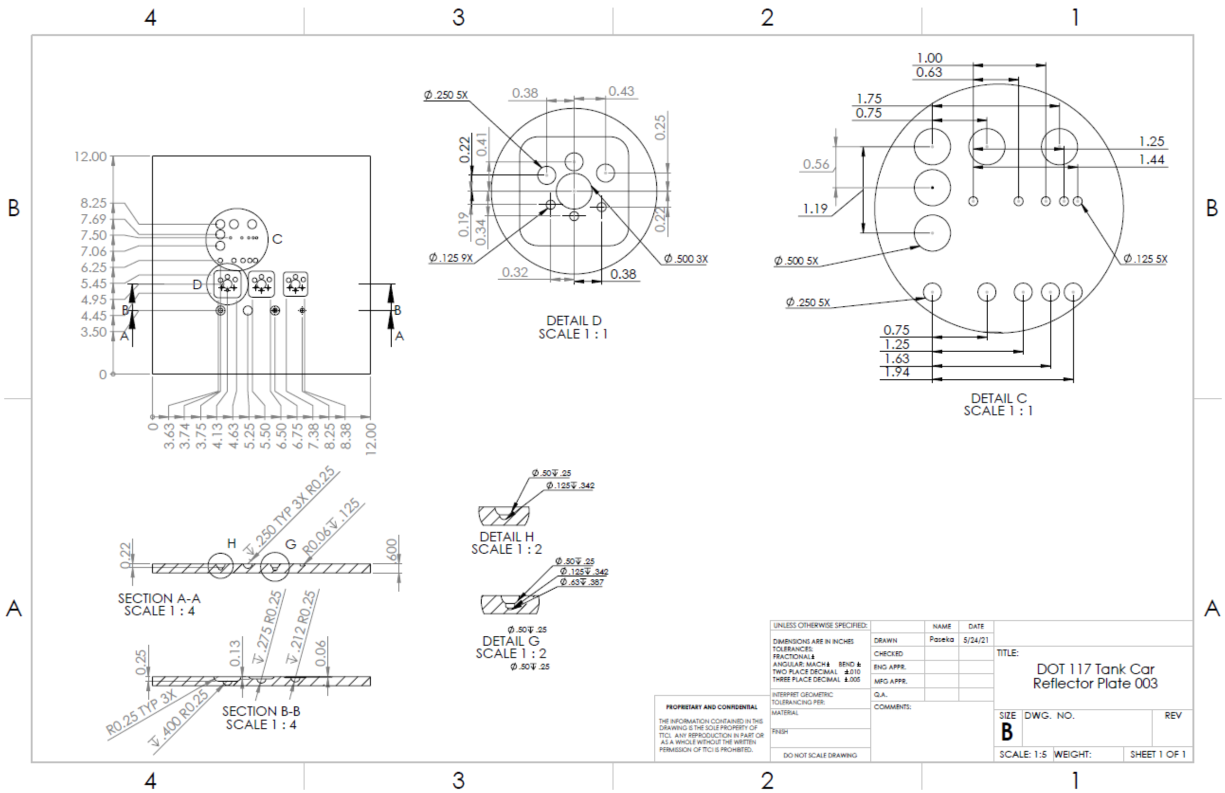

(a)

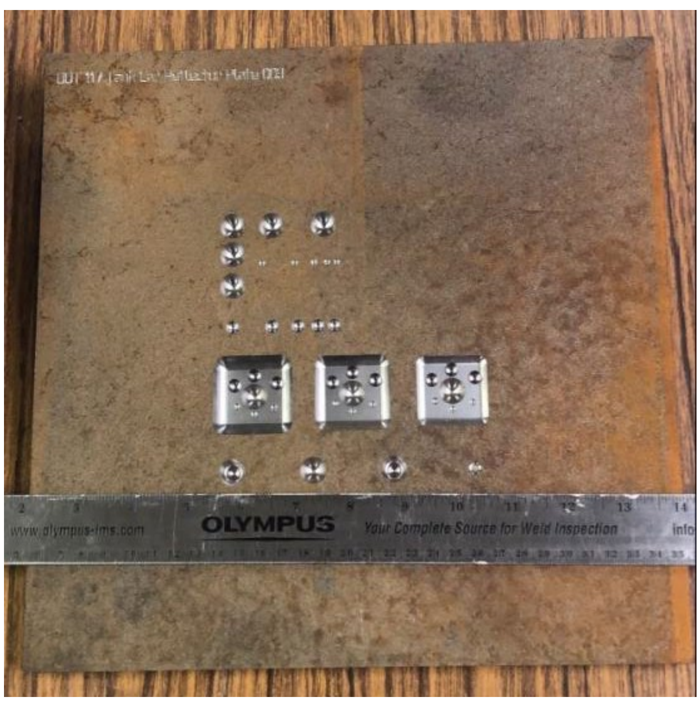

(b)

Figure 22. DOT-117 tank car corrosion reflector plate 003: (a) engineering drawing; (b) as-built part (dimension in inches)

5.3 Tank Car Corrosion Master Gauge Plates

The third round of test plates consisted of six tank car corrosion master gauge (MG) plates cut out of the DOT-117 tank car shells. These plates measure 12-inch by 24-inch, and they have artificially simulated, varied size (diameter) pits and corrosion implanted on both the inner and outer diameter of the tank shell. Table 4 lists the details of the simulated corrosion and pits for all MG plates. Similarly, Figure 23 through Figure 28 shows the engineering drawings of six tank car corrosion master gauge plates. These MG plates are designed to serve as a calibration tool for NDE capability demonstration.

Table 4. Tank car MG plates simulated corrosion and pits design specifications

MG Plates ID	Indication Types/ ID or OD	Simulated Corrosion/Pits Size (L x W X D) [inch]
MGC-1	Flaw 1 - Corrosion - OD	0.98 x 0.91 x 0.24
	Flaw 2 - Pit - ID	0.13 dia x 0.14
	Flaw 3 - Corrosion - ID	0.49 x 0.48 x 0.17
MGC-2	Flaw 1 - Corrosion - ID	1.06 x 0.91 x 0.24
	Flaw 2 - Corrosion - ID	0.47 x 0.48 x 0.13
	Flaw 3 - Corrosion - ID	0.94 x 0.93 x 0.24
MGC-3	Flaw 1 - Corrosion - OD	0.47 x 0.47 x 0.24
	Flaw 2 - Corrosion - ID	0.08 x 0.08 x 0.02
	Flaw 3 - Corrosion - ID	0.47 x 0.45 x 0.12
MGC-4	Flaw 1 - Pit - OD	0.12 dia x 0.06
	Flaw 2 - Corrosion - OD	0.24 x 0.24 x 0.13
	Flaw 3 - Corrosion - ID	1.07 x 0.98 x 0.12
MGC-5	Flaw 1 - Corrosion - ID	0.49 x 0.47 x 0.12
	Flaw 2 - Corrosion - ID	0.91 x 0.91 x 0.18
	Flaw 3 - Corrosion - OD	0.43 x 0.43 x 0.06
MGC-6	Flaw 1 - Corrosion - OD	0.24 x 0.24 x 0.02
	Flaw 2 - Corrosion - OD	0.93 x 0.91 x 0.25
	Flaw 3 - Pit - OD	0.13 dia x 0.16

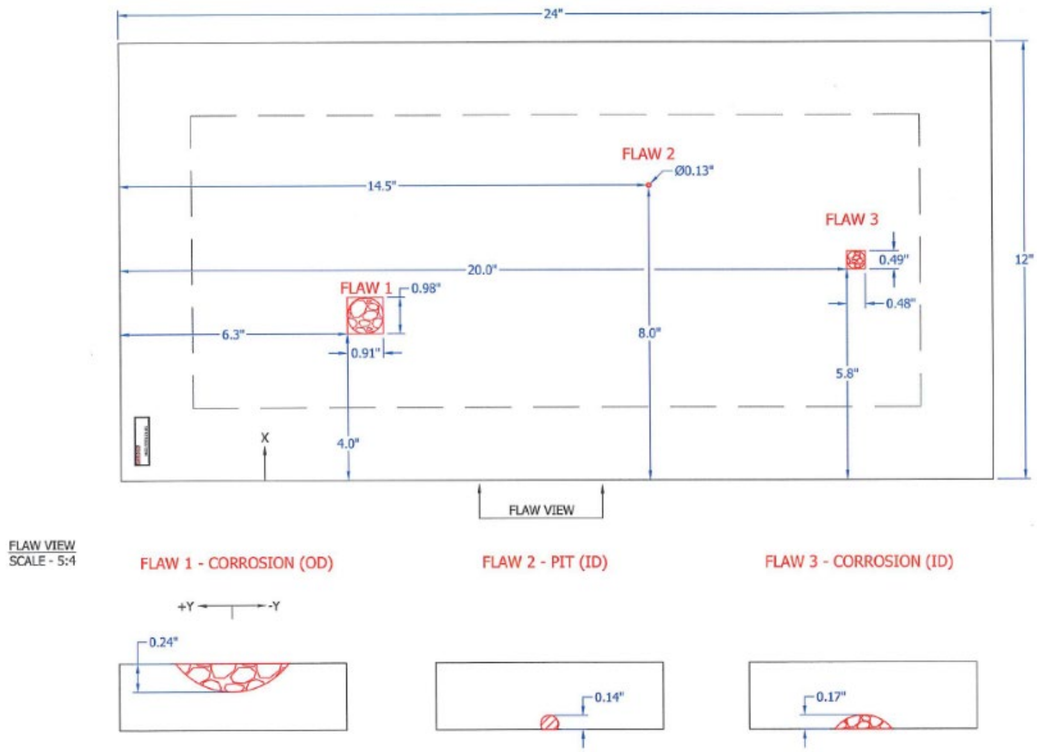

Figure 23. Engineering drawing of DOT-117 tank car corrosion MG plate MGC-1

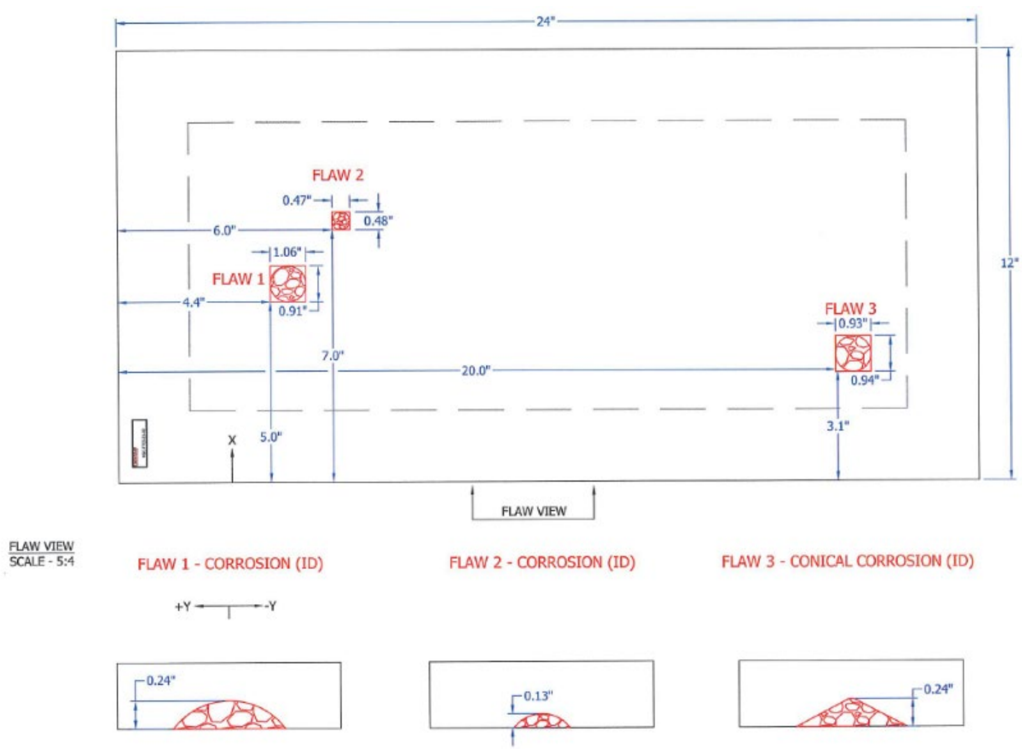

Figure 24. Engineering drawing of DOT-117 tank car corrosion MG plate MGC-2

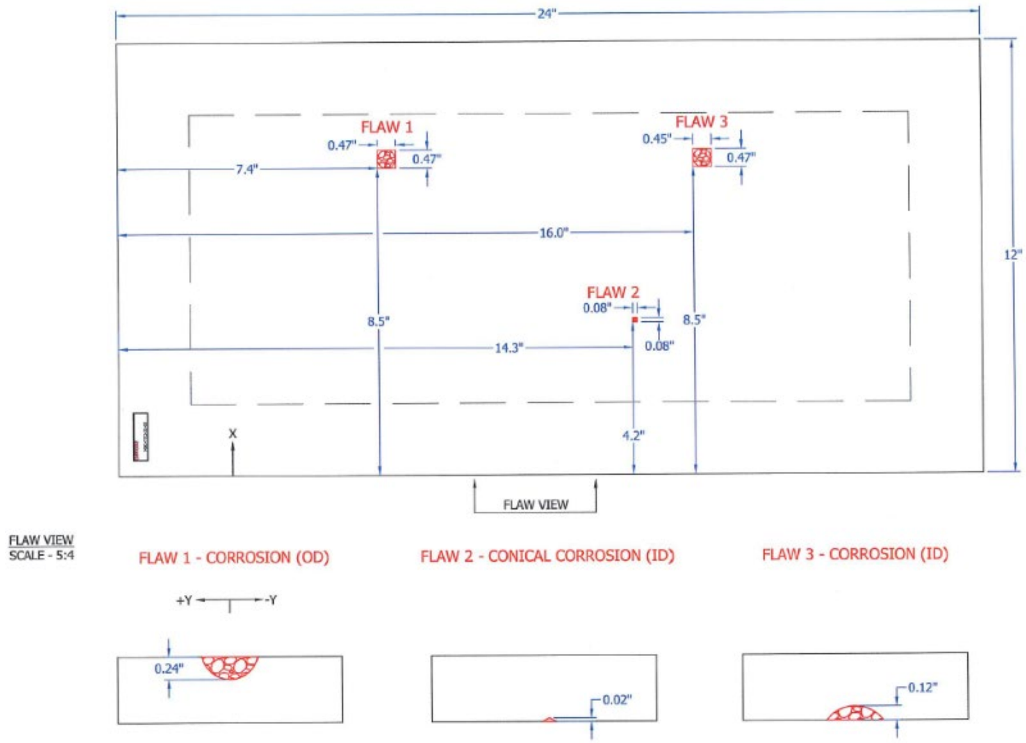

Figure 25. Engineering drawing of DOT-117 tank car corrosion MG plate MGC-3

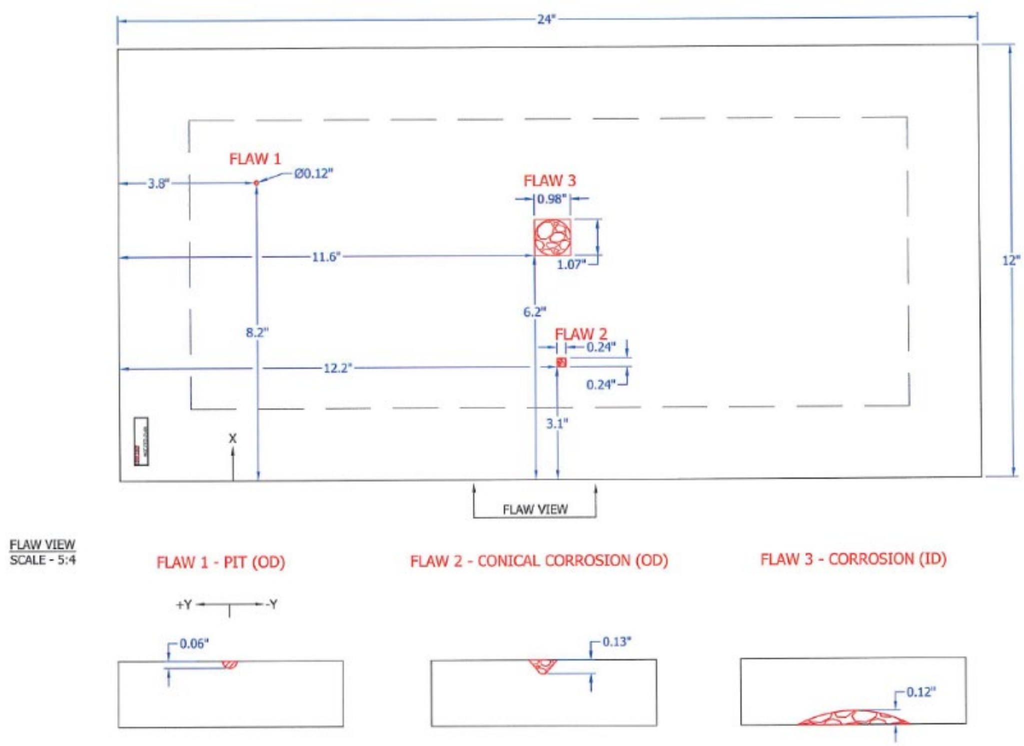

Figure 26. Engineering drawing of DOT-117 tank car corrosion MG plate MGC-4

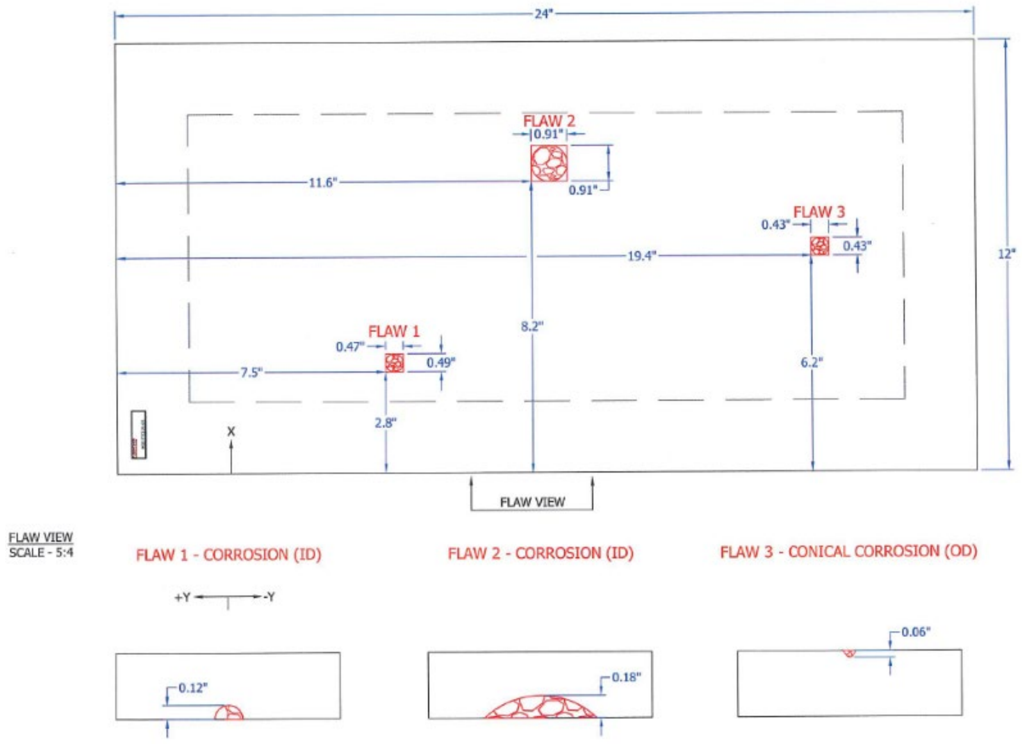

Figure 27. Engineering drawing of DOT-117 tank car corrosion MG plate MGC-5

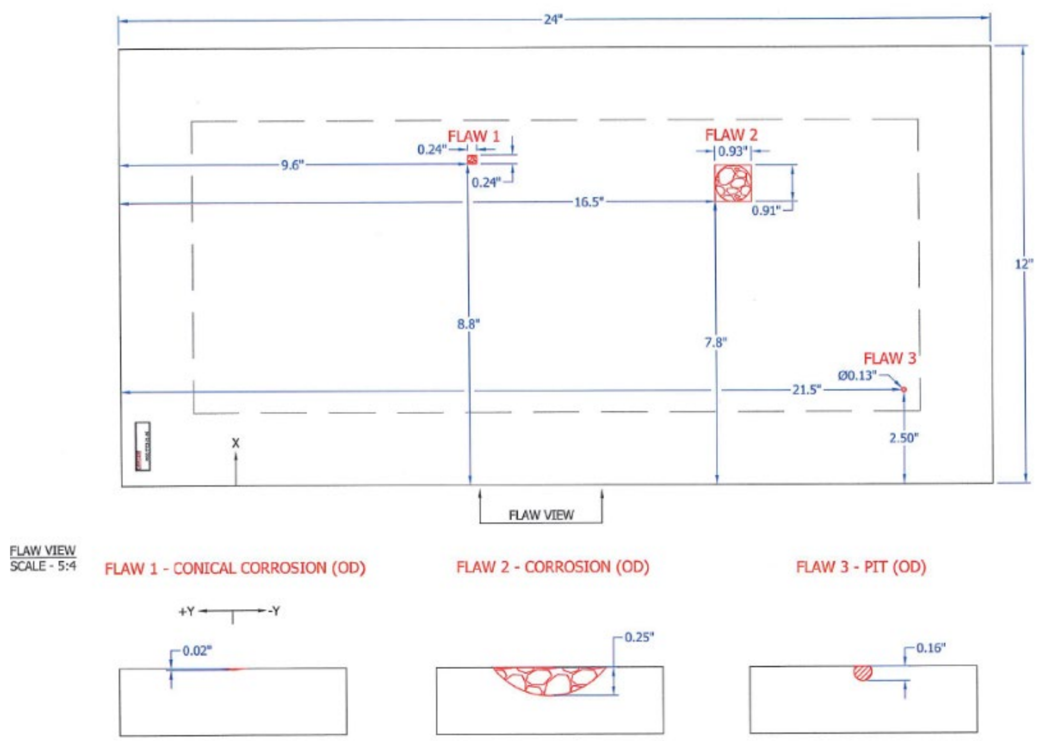

Figure 28. Engineering drawing of DOT-117 tank car corrosion MG plate MGC-6

6. NDE Trials for Corrosion Assessment

Several NDE methods were considered for this trial. While conducting this study, not all the test panels were inspected using individual techniques due to the limited availability of Original Equipment Manufacturers (OEMs) and each service provider's personnel support and time during this trial. The goal of this work was to 1) evaluate the capabilities of each applied NDE method and 2) demonstrate the feasibility to some test panels. This exercise was not meant for the capability demonstration using probability of detection (POD) metrics. A separate study 1) will be required for a full-blown POD study and 2) will require more samples to conduct the study. Some of the NDE methods considered for this trial are detailed in Sections 6.1 through 6.5.

6.1 Ultrasonic Thickness Gauge

An ultrasonic corrosion thickness gauge works by measuring the precise sound path that travels through a test piece and reflects from the back surface of the test piece. The thickness of the test piece is calculated from this measurement. The wall thickness for the test panels that were cut out of the tank cars were measured at the center of each square grid using Danatronics Echo 9, an ultrasonic corrosion thickness gauge, with a 0.25-inch diameter dual element 5 MHz transducer. A typical range for this device in corrosion mode is about 0.02-inch to 23-inch (0.508 mm to 584 mm), and the resolution is around 0.001-inches. Figure 29 shows the setup of the UTT gauge used to measure plate thickness. The thickness readings for test samples 1–7 were recorded and are presented in Table 5 through Table 11. The measurements shown along four corners in the tables for the test panel were measured with digital calipers.

Figure 29. UTT tester setup

Table 5 and Table 6 show the UT wall thickness mapping for test panel 1 and test panel 2 respectively.

Table 5. Wall thickness (inch) mapping for test panel 1

	A	B	C	D	E	F	G
1	(.4545) 0.452	0.446	0.436	0.454	0.449	0.454	(.4740) 0.470
2	0.459	0.457	0.440	0.462	0.403	0.370	0.457
3	0.458	0.464	0.450	0.454	0.462	0.452	0.437
4	0.487	0.471	0.498	0.481	0.492	0.456	0.469
5	0.505	0.504	0.463	0.478	0.466	0.486	0.463
6	0.488	0.482	0.493	0.502	0.466	0.455	0.470
7	0.479 (.4985)	0.490	0.494	0.489	0.481	0.477	0.467 (.4710)

Table 6. UT wall thickness (inch) mapping for test panel 2

	A	B	C	D	E
1	(.8010) 0.775	0.783	0.786	0.783	(.8200) 0.756
2	0.787	0.771	0.771	0.775	0.768
3	0.781	0.781	0.776	0.777	0.774
4	0.776	0.795	0.771	0.751	0.730
5	0.780	0.776	0.783	0.757	0.792
6	0.780	0.755	0.801	0.779	0.802
7	0.787 (.8460)	0.774	0.780	0.786	0.782 (.8135)

Table 7 shows the UT wall thickness mapping for test panel 3. The blank area represents areas where measurements were not possible within that 1-inch grid. Similarly, Table 8 shows the UT wall thickness mapping for test panel 4. The blank area represents areas where measurements were not possible within that 1-inch grid.

Table 7. UT wall thickness (inch) mapping for test panel 3

	A	B	C	D	E	F	G
1	(.1405) 0.159	0.156	0.147	0.149	0.150	0.148	0.146
2	0.155	0.151	0.152	0.151	0.154	0.150	0.151
3	0.154	0.154	0.154	0.146	0.135	0.151	0.153
4	0.153	0.156	0.151	0.130	0.123	0.152	0.151
5	0.174	0.160	0.164	0.165	0.152	0.152	0.153
	(0.2785)	Weld Overlap					(0.3300)
6	0.156	0.159	0.157	0.158	0.150	0.141	0.156
7	0.159	0.160	0.144	0.135	0.127	0.116	0.131
8	0.165	0.157	0.135	0.087			
9	0.164	0.159	0.156	0.130	0.143		
10	0.163	0.157	0.155	0.152	0.144	0.091	0.149
11	(.1405)	0.160	0.168	0.159	0.154	0.144	(.1440) 0.146

Table 8. UT wall thickness (inch) mapping for test panel 4

	A	B	C	D	E	F	G	H	I	J	K
1	(.1015) .118	0.104	0.091	0.075		0.068	0.070	0.075	0.068	0.077	(.1135) 0.098
2						0.065	0.085	0.110	0.101	0.050	0.095
3	0.051	0.052	0.057	0.055				0.060	0.090	0.113	0.095
4	0.055	0.074	0.061	0.064	0.078	0.052		0.085	0.116	0.128	0.121
5	0.097	0.089	0.088	0.055	0.100		0.062	0.079	0.107	0.127	0.116
6	0.088	0.078	0.075	0.074	0.094	0.050	0.050	0.101	0.107	0.098	0.081
7	0.087	0.076	0.086	0.072	0.065	0.069	0.056	0.071	0.091	0.090	0.071
8	0.102	0.094	0.091	0.075	0.072	0.054	0.097	0.051	0.077	0.099	0.100
9	0.090	0.093	0.100	0.067	0.052	0.058	0.068		0.060		
10	0.091	0.089	0.094	0.062	0.092	0.067	0.086	0.078	0.051		
11	(.0890) .095	0.066	0.105	0.065	0.083	0.066	0.094	0.078	0.049		(0.0440)

Table 9 shows the UT wall thickness mapping for test panel 5. The blank areas represent measurements that were unavailable within that 1-inch grid.

Table 9. UT wall thickness (inch) mapping for test panel 5

	A	B	C	D	E	F	G	H	I	J	K	L	M	N	O	P
	(0.0935)			(0.1185)				(0.0710)				(0.088)				(0.110)
1	0.088						0.113	0.105	0.115	0.086	0.114	0.082	0.105	0.111	0.109	0.112
2	0.079	0.067	0.076	0.094	0.088	0.119		0.083	0.118	0.080	0.081	0.057	0.077	0.094	0.113	0.126
3	0.089	0.051	0.066	0.066	0.061				0.109	0.090	0.077	0.122	0.104	0.067	0.095	0.110
4	(0.0800) 0.074	0.051	0.051	0.064					0.099	0.090				0.071	0.087	(0.1050) 0.095
5	0.074	0.059	0.060		0.064			0.061	0.118	0.080					0.061	0.085
6	0.077	0.067			0.048	0.055	0.086	0.069	0.101	0.051	0.077					0.102
7	0.062	0.061									0.094	0.111				0.098
8	0.067	0.056			0.095							0.086				0.113
9	0.079					0.101		0.130	0.090		0.081	0.084				0.102
10	0.082	0.094				0.075			0.060	0.089	0.066	0.091				0.109
11	0.078	0.048				0.058			0.073		0.113				0.103	0.103
12	(0.0980) 0.101	0.070	0.058			0.077	0.059		0.123	0.109	0.090					(0.1200) 0.119
13	0.104	0.105	0.079	0.063					0.111	0.072					0.104	0.123
14	0.102	0.110	0.077	0.076		0.103	0.079	0.045	0.121	0.101				0.079	0.125	0.126
15	0.104	0.077	0.107	0.090	0.060	0.072			0.121	0.110	0.062		0.051	0.118	0.125	0.127
16	(0.1315) 0.109	0.110	0.111	0.087	0.055	0.089	0.078	0.100	0.124	0.108	0.085	0.076	0.100	0.129	0.131	(0.1280) 0.133
17	0.109	0.102	0.116	0.111	0.110	0.088	0.096	0.053	0.133	0.106	0.086	0.094	0.123	0.136	0.135	0.137
18	0.109	0.104	0.116	0.113	0.112	0.102	0.092	0.087	0.130	0.106	0.076	0.095	0.125	0.137	0.134	0.133
19	(0.1245) 0.125	0.127		(0.1025)				(0.0970)				(0.1125)	0.135		0.137	(0.1275) 0.135

Table 10 shows the UT wall thickness mapping for test panel 6. The blank area represents areas where measurements were not possible within that 1-inch grid.

Table 10. UT wall thickness (inch) mapping for test panel 6

	A	B	C	D	E	F	G	H	I	J	K	L	M	N	O	P	Q
1	0.191	0.166	0.180			(0.0740)	0.180			0.058	(.0620) .062	0.094		0.156			(.1100) .153
2						0.088				0.060	0.073						0.099
3								0.089	0.053	0.082	0.094						0.117
4	0.108							0.096	0.048	0.064	0.100					0.113	0.110
5									0.071	0.062	0.098						(.1285) .125
6	0.099			(0.0890)					0.072	0.074	0.076	0.098		0.098	0.086	0.073	0.127
7														(.0830) .095	0.098	0.113	0.113
8															0.100	0.120	0.119
9															0.125	0.130	0.117
10						0.066	0.053	0.119							0.102	0.114	(.1635) .100
11	0.088	0.111		0.105	0.102	0.093	0.086	0.091	0.103	0.101				0.123	0.126	0.124	0.128
12	0.112	0.110	0.111	0.115	0.113	0.114	0.105	0.116	0.118	0.124				0.124	0.131	0.138	0.131

	A	B	C	D	E	F	G	H	I	J	K	L	M	N	O	P	Q	
13	0.123	0.115	0.126	0.124	0.119	0.115	0.109	0.116	0.101	0.132					0.112	0.121	0.112	0.111
14	0.127	0.124	0.128	0.130	0.123	0.106	0.110	0.098	0.115	0.123				(0.0980)	0.131	0.111	0.119	0.099
15	0.129	0.131	0.130	0.136	0.112	0.127	0.101	0.100	0.105	0.128					0.109	0.099	0.115	0.124
16	0.052	0.052						0.112	0.119						0.116	0.109	0.117	0.103
17	(.1205) .100	0.095					0.110	0.093	0.073	0.115	0.104				(.1050) .097	0.120	0.123	(0.1525)
18		0.106	0.074		0.092	0.105	0.118	0.095	0.090	0.124	0.123					0.107	0.130	0.129
19	0.078	0.085	0.065		0.061	0.064	0.125	0.120	0.106	0.144	0.100					0.109	0.125	0.130
20	(.1270) .116	0.115	0.108	0.115	0.127	0.115	0.116	0.130	0.167		0.113	0.145				0.127	0.125	(.1380) .132
21	0.113	0.106	0.114	0.105	0.111	0.092	0.107	0.112	0.128		0.122	0.131			0.122	0.123	0.125	0.122
22	0.111	0.114	0.104	0.107	0.111	0.102	0.094	0.112	0.153		0.100	0.123	0.095	0.116	0.109	0.115	0.123	0.133
23	0.116	0.108	0.113	0.118	0.124	0.107	0.097	0.112	0.116	0.140	0.116	0.125	0.079	0.064	0.117	0.125	0.132	0.134
24	(.1370) .116	0.118	0.107	0.118	(.1220) .106	0.103	0.102	0.118	0.109		(.1085) .120	0.146	0.094	0.105	(.1335) .125	0.102	0.130	(.1460) .132

Table 11 shows the UT wall thickness mapping for test panel 7. The blank areas represent areas where measurements were not possible within that 1-inch grid.

Table 11. UT wall thickness (inch) mapping for test panel 7

		1	2	3	4	5	6	7	8	9	10	11	12	13	14	15	16	17	18	19	20	21	22	23	24	25	26	27	28	29	30	31	32	33	34	
		(0.1365)	0.115			0.124	(0.1450)	0.116			(0.1495)				(0.1595)			(0.1460)											(0.1265)							
1	A	0.116	0.123			0.120	0.111	0.127	0.121	0.122	0.120	0.138	0.177	0.140	0.135	0.126	0.137	0.140	(.1255) .130	0.138	0.142	(.1565) 0.158	0.152	0.128	(.1315) .159	0.147		0.162	0.130	0.131	0.130		0.126	0.127	0.130	(0.2915)
2	B	(.1280) .120	0.125			0.129	0.129	0.112	0.123	0.116	0.126	0.125	0.130	0.127	0.132			0.129	0.108		0.149				0.133	0.142		0.164		0.118	0.124	0.124	0.135	0.129	0.136	
3	C	0.119	0.125			0.134	0.129	0.124	0.134	0.131	0.129	0.128	0.130	0.120	0.132		0.137	0.149		0.127		0.129	0.152	0.144	0.128	0.123	0.113	0.124	0.125	0.131	0.127	0.134	0.139	0.131		
4	D	0.124	0.126			0.117	0.129	0.129	0.130	0.133	0.126	0.120	0.124	0.127	0.130	0.115	0.121	0.129	0.132	0.128	0.130	0.136	0.144	0.144	0.130	0.110	0.112	0.130	0.124	0.129	0.129		0.151	0.137		
5	E	(.1355) .127	0.127			0.125	0.132	0.129	0.126	0.127	0.125	0.119	0.134	0.132	0.125	0.122	0.126	0.122	0.125	0.126	0.130	0.127	0.111	0.136	0.132	0.116	0.128	0.109	0.117	0.113	0.125	0.126	0.130	0.134	0.131	
6	F	0.120	0.122			0.113	0.130	0.138	0.130	0.126	0.132	0.117	0.120	0.121	0.123	0.122	0.127	0.127	0.140	0.127	0.140	0.131	0.128	0.132	0.151	0.131	0.139	0.114	0.126	0.122	0.130	0.127	0.125	0.122	0.150	(0.3035)
7	G	0.123	0.124			0.125	0.131	0.112	0.131	0.131	0.123	0.119	0.128	0.111	0.120	0.131	0.136	0.135		0.123	0.131	0.128	0.141	0.138	0.124	0.134		0.125	0.128	0.127	0.126	0.138	0.130	0.130	0.116	
8	H	0.123	0.113		0.129	0.130	0.135	0.127	0.129	0.112	0.123	0.123	0.127	0.123	0.133	0.160	0.135	0.135	0.131	0.166	0.134	0.147	0.129	0.129	0.161		0.133	0.074	0.115	0.136	0.134	0.135	0.134	0.128	0.123	
9	I	(.1285) .118	0.128		0.138	0.126	0.127	0.126	0.127	0.125	0.116	0.112	0.130	0.136	0.120	0.168	0.115	0.128	0.150	0.122	0.140	0.111	0.103	0.124		0.130	0.101	0.132	0.105	0.127		0.133	0.137	0.123	0.112	
10	J	0.116	0.125			0.128	0.132	0.144	0.132	0.137		0.140	0.130	0.111	0.113	0.128	0.130	0.129	0.123	0.142	0.170	0.143	0.117				0.115	0.144	0.128			0.137	0.129	0.128	0.141	
11	K	0.125	0.114			0.137		0.151	0.132		0.105	0.128	0.131	0.114	0.150	0.117		0.142	0.126	0.139			0.122	0.107				0.127	0.121	0.117				0.125	0.119	(0.1295)
12	L	(1470) 0.125	0.127				0.167		0.129		0.135		0.145		0.145	0.155	0.125	0.134	0.131	0.135	0.144	0.134	0.122			0.087		0.129	0.107	0.131		0.165	0.136	0.129	0.130	
13	M	0.116	0.122	0.123	0.127	0.129	0.138	0.125		0.120			0.168				0.111	0.152			0.156					0.118			0.141	0.147		0.130	0.157	0.133	0.135	
14	N	0.092	0.118	0.122	0.127	0.121	0.120	0.110	0.113	0.109	0.114	0.115	0.121				0.123	0.121	0.115	0.120					0.114			0.143	0.123	0.114	0.121	0.124	0.158	0.095	0.123	
15	O	(.1260) 0.115	0.122	0.122	0.126	0.121	0.127	0.101	0.105	0.115	0.124	0.124	0.127	0.124	0.125	0.101	0.111	0.103	0.121	0.126	0.123	0.125	0.125	0.126	0.132	0.130	0.111	0.129	0.128	0.126	0.126	0.129	0.125	0.109	0.120	(0.1280)
16	P	0.103	0.121	0.122	0.127	0.120	0.119	0.106	0.112	0.125	0.127	0.127	0.114	0.112	0.113	0.119	0.115	0.117	0.121	0.127	0.123	0.127	0.111	0.094	0.128	0.138	0.098	0.129	0.112	0.121	0.130	0.125	0.110	0.109	0.119	
17	Q	(.1345) 0.114	0.104	0.107	0.125	0.122	0.115	0.125	0.108	0.125	0.124	0.127	0.123	0.114	0.122	0.119	0.118	0.119	0.123	0.122	0.104	0.120	0.093	0.117	0.098	0.122	0.121	0.109	0.118	0.096	0.111	0.127	0.137	0.110	0.122	
18	R		0.112	(.1240) .122	0.126	0.115	(.1540) .111	0.120	0.126	0.124	0.124	0.125	0.126	0.121	0.114	0.115	0.121	0.113	0.128	0.126	0.105	0.122	0.089	0.124	0.125	0.117	0.072	0.114	0.119	0.112	0.122	0.125	0.114	0.115	0.123	
19	S										(0.1325)	0.125	0.127	0.120	(1310) .122	0.122	0.123	(.1495) .117	(.1360) .121	0.128	0.126	(.1230) 0.127	0.119	0.112	(.1460) .105	0.092	(.1470) .118	0.122	0.121	0.116	0.108	(.1520) .122	0.104	0.123	0.123	(0.1180)

6.2 Phased Array Ultrasonic Testing

PAUT is an advanced ultrasonic NDE method that uses multiple elements (transducers) in a single probe housing with the capability to send an array of sound, in a wide range of angles, through the material being tested. The main advantage of the PAUT method is that it uses multiple elements within a single transducer assembly to steer, focus, and scan beams, which reduces inspection times and improves productivity. A larger aperture of the PAUT probe will allow to map the variations in material thickness due to corrosion at higher speeds and help to graphically plot the problematic locations. PAUT is widely used today for the in-service detection and characterization of corrosion in pipelines, tanks, pressure vessels, marine vessels, and other critical assets.

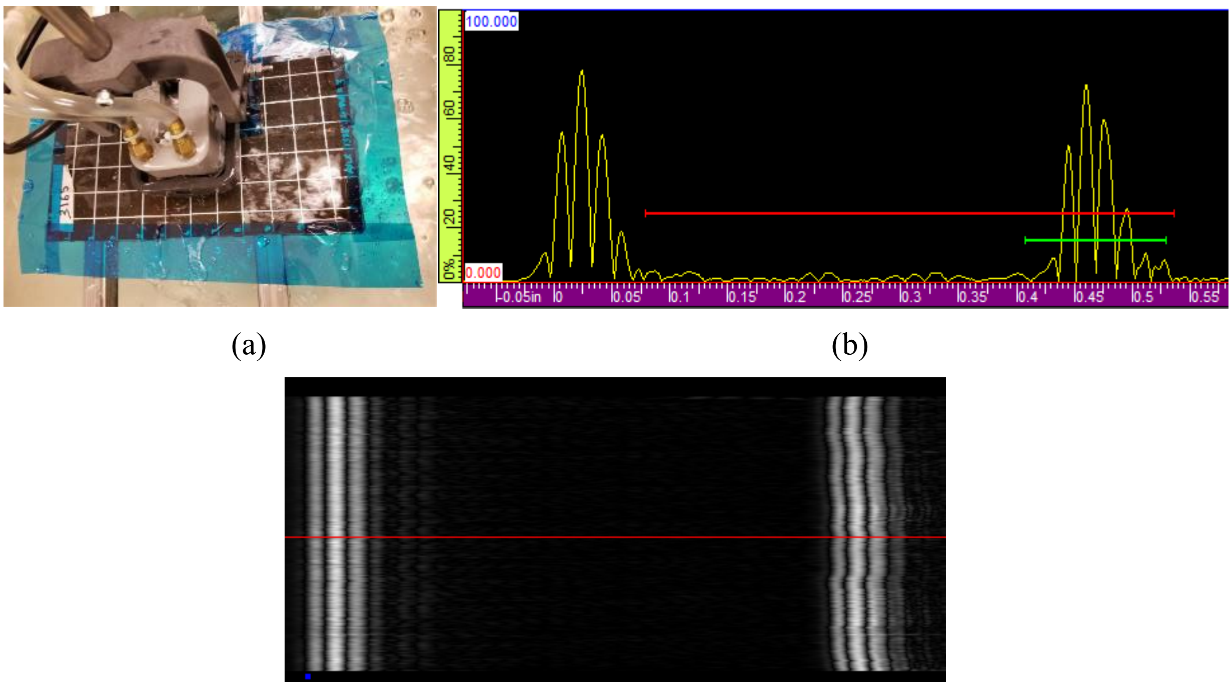

(a) (b)

(c)

Figure 30. PAUT setup for corrosion monitoring: (a) bubbler NDE system; (b) A-scan signal on a good section; (c) corresponding B-scan on a good section

To test the feasibility of the PAUT method, the technician used an automated bubbler NDE system to simulate immersion. The PAUT transducer was mounted in a bubbler shoe for water coupling, and the water path distance was set at 1 inch. A 3.5 MHz 2-inch cylindrical focus PAUT transducer (96 elements) was used for this work. Samples were taped around the edges before the inspection to prevent water from gathering on the back surface. All parts were inspected from the outer diameter (convex) surface with scan resolution of 0.04-inches, and all C-scans were encoded using an X-Y scan bridge. Figure 30 shows the experimental test setup used for this study. Figure 31 shows the amplitude and time of flight C-scan results for the three corrosion plates. Although, the corrosion in the test panels could be mapped, these test coupons presented significant inspection challenges because both the front and back surfaces were uneven, rough, and corroded.

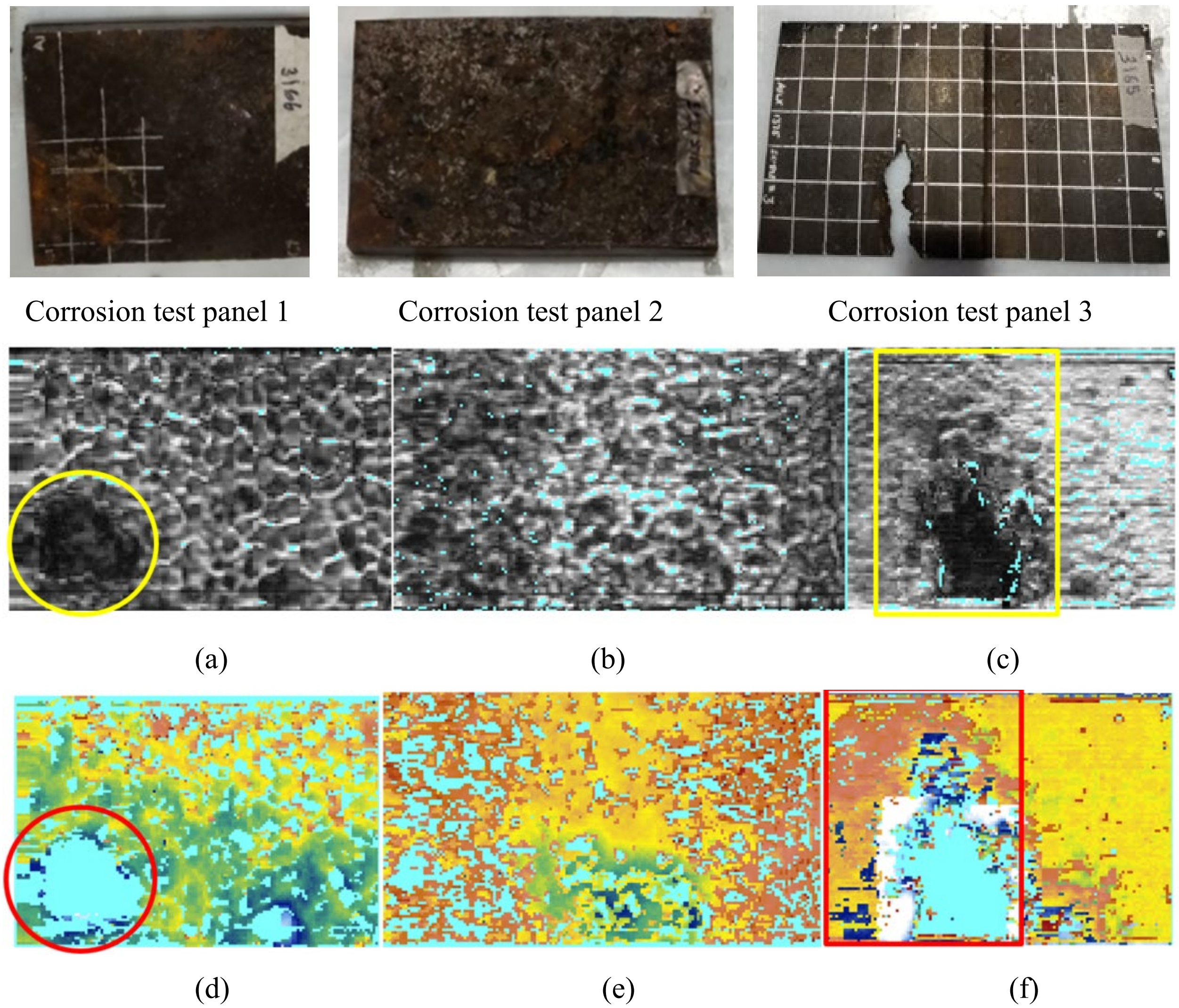

Figure 31. PAUT C-scan results: (a–c) Amplitude C-scan images; (d–f) Time of Flight (TOF) C-scan images

Beside corrosion plates, previously built DOT-111 fillet welds (FW), butt welds (BW), and MG plates were also inspected. Figure 32 to Figure 34 show the C-scan results (amplitude and TOF) for MGL-9, MGL-3, and MG-6 plates. These scan results show the thickness of the part at different areas that can be determined successfully using this approach. For the MGL-3 plate, it is evident from the C-scans that the front and back surface signal amplitude changes significantly on sections of the panel with and without paint/coatings. Similarly, for the MG-6 plate, the thickness change near the BW (marked 1 and 2) indicates the location of simulated fatigue cracks that were buffed to mask the cracks at the toe of the weld, and this was also evident in the TOF C-scan image results which was encouraging.

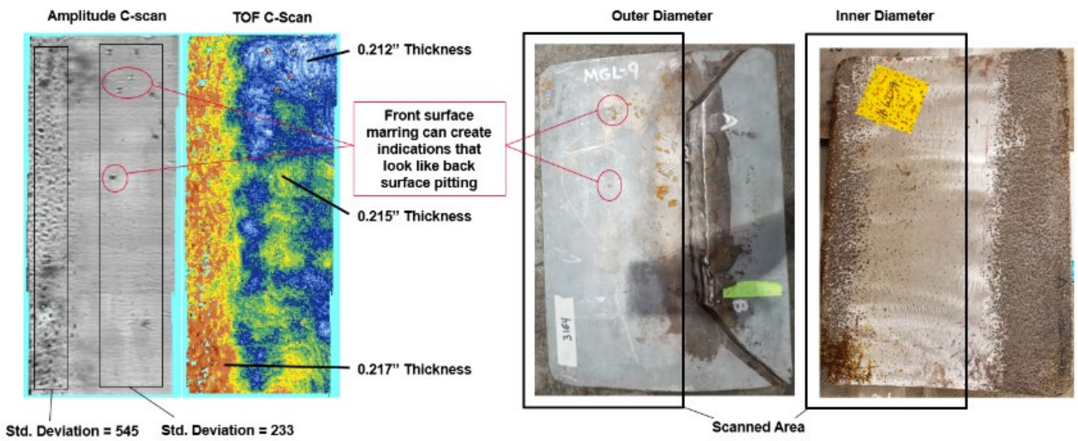

Figure 32. DOT-111 MGL-9 FW plate C-scan result

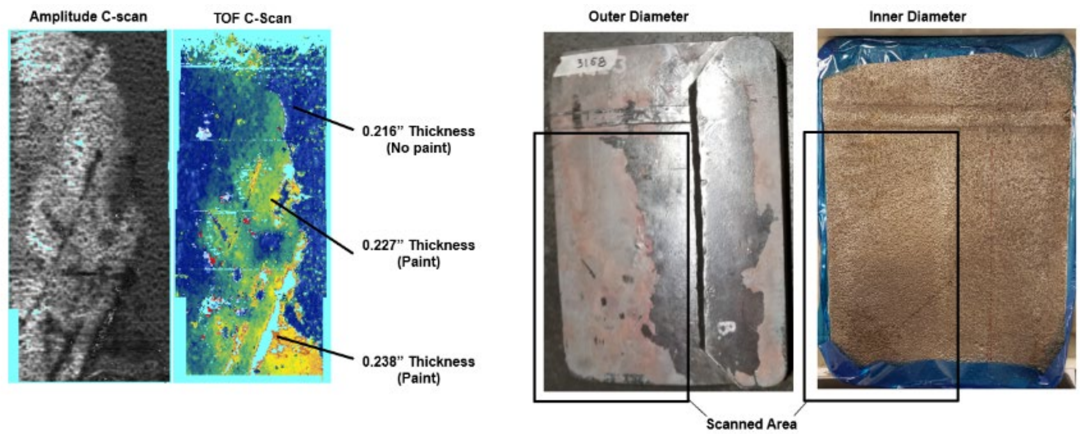

Figure 33. DOT-111 MGL-3 FW plate C-scan result

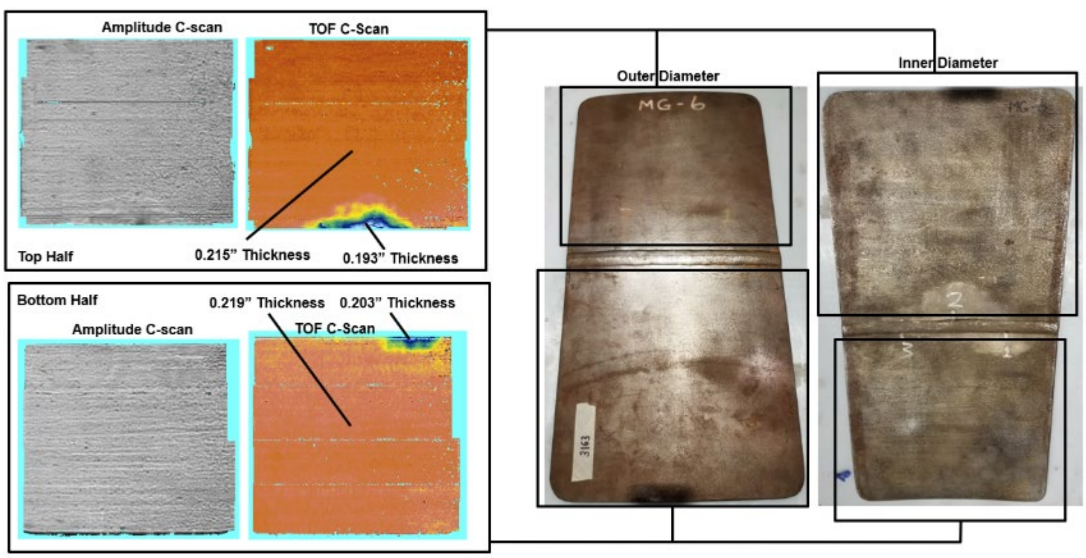

Figure 34. DOT-111 MG-6 BW plate C-scan result

6.3 Backscatter X-Ray Imaging

Backscatter X-ray imaging is one of the radiography NDE techniques where both the X-ray source and detector are on the same side of the target and use rotating collimators, which pass through a slit and are swept across an object of interest, to generate X-rays in a motion profile appropriate for covering the area of interest [50]. This technique allows the capture of the spatial density distribution of an object by irradiating it with X-rays and then measuring the intensity distribution of scattered X-rays [51, 52]. Several advantages to using this method include:

1. Non-contact and does not require surface preparation or any coupling
2. Detect a crack and corrosion below the surface through thick insulations
3. Not susceptible to surface roughness and material properties, except their densities
4. Not require two-sided access, enabling testing of large extended structures

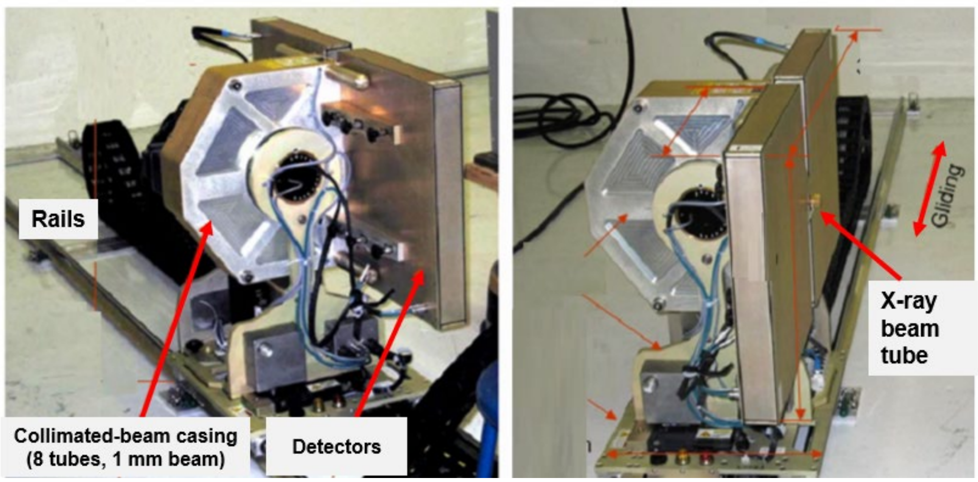

Figure 35. Backscatter X-ray imaging system

The backscatter X-ray imaging considered for this was a real-time imaging modular mobile system that required no films to collect images. It used two adjustable detectors (± 0-degree tilt capable) to measure the backscatter signal and eight-beam tubes housed in collimated beam casing. The collimator design and aperture can be adjusted in different directions and for different applications. The maximum power can be achieved at 220 KeV and 11.2 mV. Figure 35 shows the backscatter X-ray system that was used to inspect tank car panels. Figure 36 shows the test setup where a thick insulation was placed in front of the test panel to simulate a real-world situation that the scanner needs to go through to scan the tank car shell.

Figure 37 and Figure 38 show the backscatter X-ray imaging of the tank car corrosion test panels where the areas of material loss and corrosion can be seen visually in the scan results, thereby proving the capability of this method to image corrosion in tank car through insulation. More work needs to be conducted to fully understand the capability and limitations of such technology.

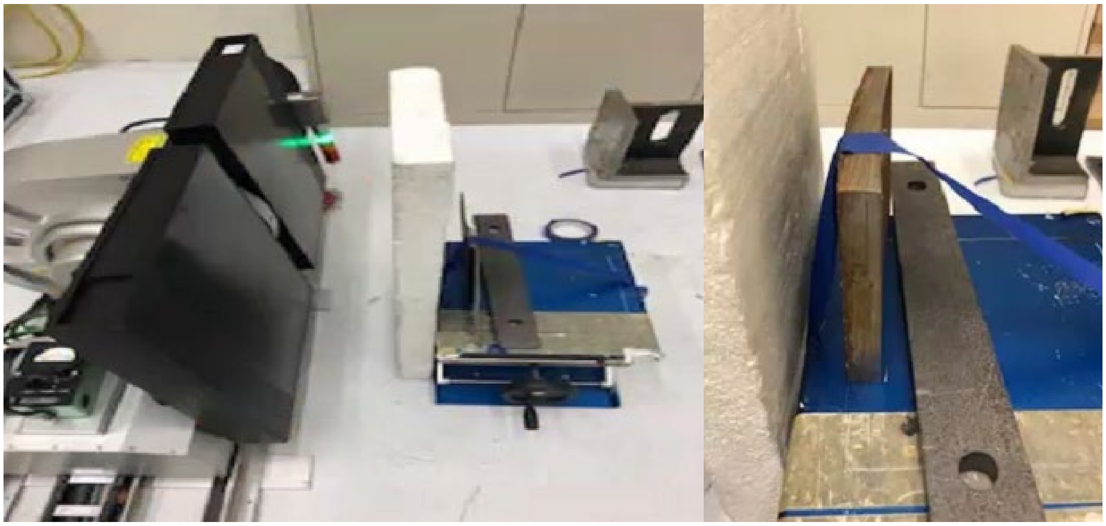

Figure 36. Backscatter X-ray system inspection setup through 2-inch ridged insulation

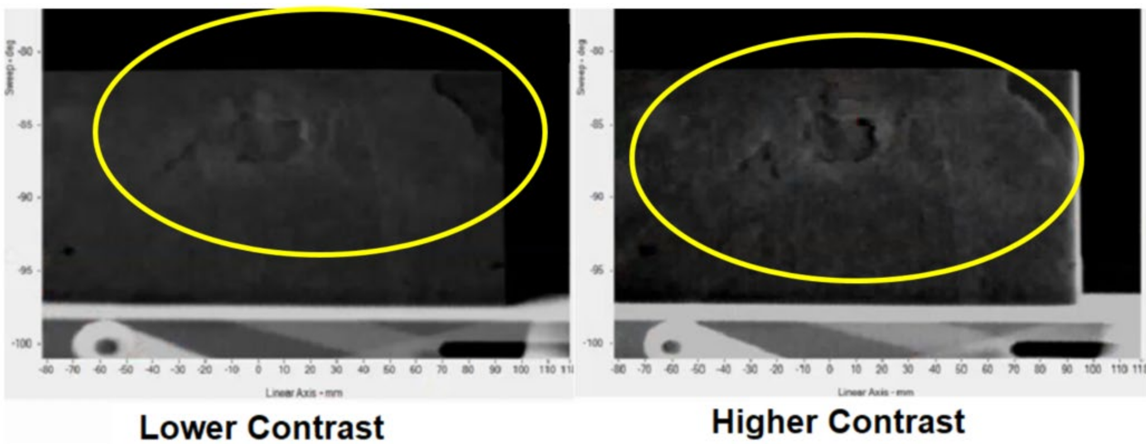

Figure 37. Backscatter X-ray imaging result for corrosion test panel 1

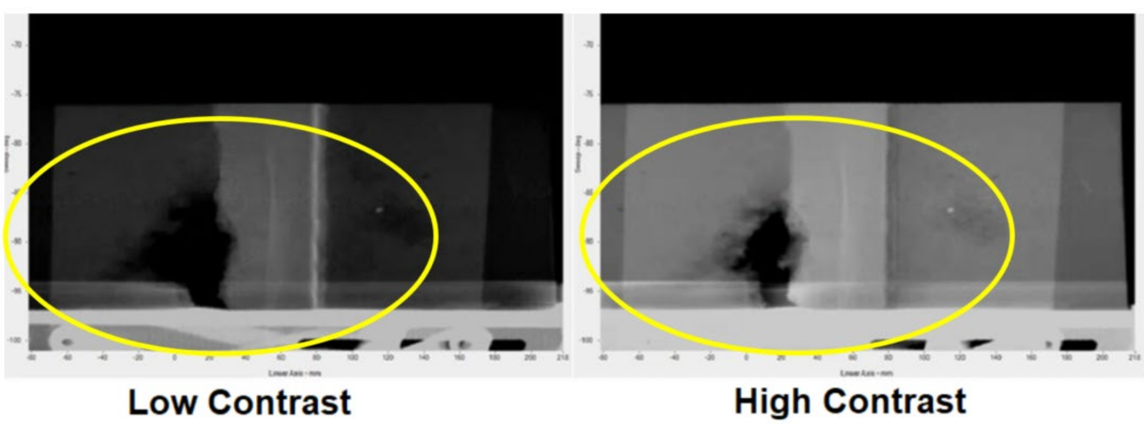

Figure 38. Backscatter X-ray imaging result for corrosion test panel 3

6.4 Electro Magnetic Acoustic Transducers

EMATs are a non-contact NDE method that does not require a couplant to perform the inspection, as the ultrasound is generated directly within the material adjacent to the transducer. EMAT ultrasound generation is based on the interaction between the magnetic field created by a magnet and the eddy currents induced in the test piece by a coil circuit. The combination creates a Lorentz force within the material, a force that causes vibrations of the material's lattice, thereby generating ultrasonic waves [53]. Long-Range UT (LRUT) has been used for many years to rapidly inspect pipelines for corrosion, erosion, and other types of degradation using ultrasonic guided waves for further evaluation using other NDE methods. The large blind zone, limited resolution, and complex interpretation, however, make it difficult for this application to be used on the field [35]. An EMAT-generated Medium-Range UT (MRUT) has been developed to address these limitations and provide a robust and proven solution to the problem. The MRUT technique permits scanning very large/hidden areas from one location to find potential problems without having to set the probe on top. However, it is not a sizing technique, it is strictly a technique to find corrosion and flaws.

Due to the smaller sample size of corrosion panels, the MRUT technique could not be applied to evaluate the test panels. Instead, a standard single-channel EMAT system with spiral shaped sensor with a 1-inch diameter at a frequency of 2 MHz generating a shear horizontal (SH) normal beam was used for the evaluation. The shear wave velocity was kept fixed at 0.126 inch/µsec. These settings allowed the achievement of a stable signal with less attenuation. The Time of Flight (TOF) measurements were conducted as absolute time for the highest "PEAK" in the gate. The measurements were performed per the marked grid where panel-1 and panel-2 provided valid backwall signals for all measurement points, however, panel-3 (tank jacket) provided no measurement in few of the grid spots due to very low (almost none) amplitude stemming from excessive signal scattering due to heavy corrosion. Figure 39 shows a typical A-scan signal collected for sample 1 at position A1.

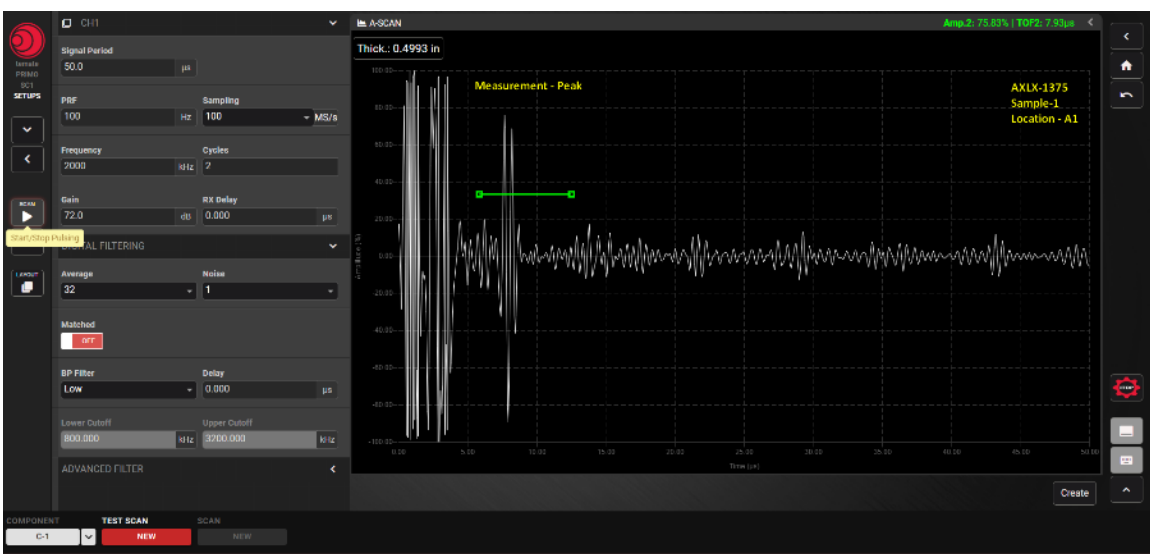

Figure 39. Typical A-scan recorded in the corrosion test panel 1

Table 12 shows EMAT thickness results for corrosion test panel 1. Cells E2 and F2 identified as having a loss of wall and validated with UTT measurements. Table 13 shows the EMAT and UTT differences in the results for test panel 1.

Table 12. EMAT thickness reading for carrion test panel 1

	A	B	C	D	E	F	G
1	0.4993	0.4781	0.4737	0.4866	0.4162	0.4775	0.4932
2	0.4970	0.4721	0.4702	0.5076	0.4911	0.4558	0.5005
3	0.4810	0.4838	0.4843	0.4845	0.4885	0.4992	0.4809
4	0.5286	0.5232	0.4952	0.5254	0.5121	0.5027	0.4918
5	0.5270	0.5340	0.5161	0.5335	0.4912	0.4959	0.4905
6	0.5397	0.4886	0.5110	0.5297	0.4890	0.4680	0.4932
7	0.5186	0.5235	0.5423	0.5502	0.5324	0.5010	0.4768

Table 13. EMAT and UTT reading difference for corrosion test panel 1

	A	B	C	D	E	F	G
1	0.0473	0.0321	0.0377	0.0326	-0.0328	0.0235	0.0232
2	0.0380	0.0151	0.0302	0.0456	0.0881	0.0858	0.0435
3	0.0230	0.0198	0.0343	0.0305	0.0265	0.0472	0.0439
4	0.0416	0.0522	-0.0028	0.0444	0.0201	0.0467	0.0228
5	0.0220	0.0300	0.0531	0.0555	0.0252	0.0099	0.0275
6	0.0517	0.0066	0.0180	0.0277	0.0230	0.0130	0.0232
7	0.0396	0.0335	0.0483	0.0612	0.0514	0.0240	0.0098

Table 14 shows EMAT thickness results for corrosion test panel 2. This panel had general corrosion and thickness loss over the entire area. Table 15 shows the differences in the thickness reading results for test panel 2.

Table 14. EMAT thickness reading for carrion test panel 2

	A	B	C	D	E
1	0.8040	0.8115	0.7968	0.8076	0.7869
2	0.8054	0.8092	0.7875	0.8062	0.7889
3	0.8152	0.8143	0.7951	0.8063	0.8091
4	0.8091	0.8097	0.8069	0.7794	0.7678
5	0.7982	0.8073	0.7877	0.7806	0.8033
6	0.8100	0.7936	0.7998	0.7913	0.8081
7	0.8135	0.8369	0.8061	0.7947	0.7961

Similarly, Table 16 shows the results for corrosion test panel 3. Blanks in the table represent areas where the technology was unable to achieve a result due to the material wall being too thin or being corroded away. Table 17 shows the differences in the results for sample 3. There is a larger difference in results compared to the previous two samples due to the sample being thinner and with heavy corrosion.

Table 15. EMAT and UTT reading difference for corrosion test panel 2

	A	B	C	D	E
1	0.0290	0.0285	0.0108	0.0246	0.0309
2	0.0184	0.0382	0.0165	0.0312	0.0209
3	0.0342	0.0333	0.0191	0.0293	0.0351
4	0.0331	0.0147	0.0359	0.0284	0.0378
5	0.0182	0.0313	0.0047	0.7049	0.0113
6	0.0300	0.0386	-0.0012	0.0123	0.0061
7	0.0265	0.0629	0.0201	0.0087	0.0141

Table 16. EMAT thickness reading for carrion test panel 3

	A	B	C	D	E	F	G
1	0.1137	0.1139	0.1133	0.1136	0.1135	0.1137	0.1131
2	0.1142	0.1139	0.1136	0.1133	0.1134	0.1138	0.1135
3	0.1140	0.1136	0.1139	0.1134		0.1132	0.1132
4	0.1135	0.1121	0.1058		0.1046	0.1102	0.1128
5	0.1131		0.1065		0.1014	0.1093	0.1073
6	0.1138	0.1134	0.1138	0.1124	0.1053		
7	0.1143	0.1153		0.0906			
8	0.1153	0.1150	0.0663				
9	0.115	0.115	0.114				
10	0.115	0.115	0.114	0.114	0.112	0.097	0.107
11	0.1149	0.1143	0.1143	0.1145	0.1142	0.1130	0.1120

Table 17. EMAT and UTT reading difference for corrosion test panel 3

	A	B	C	D	E	F	G
1	-0.0453	-0.0421	-0.0337	-0.0354	-0.0365	-0.0343	-0.0329
2	-0.0408	-0.0371	-0.0384	-0.0377	-0.0406	-0.0362	-0.0375
3	-0.0400	-0.0404	-0.0401	-0.0326		-0.0378	-0.0398
4	-0.0395	-0.0439	-0.0452		-0.0184	-0.0418	-0.0382
5	-0.0609		-0.0575		-0.0506	-0.0427	-0.0457
6	-0.0422	-0.0456	-0.0432	-0.0456	-0.0447		
7	-0.0447	-0.0447		-0.0444			
8	-0.0497	-0.0420	-0.0687				
9	-0.0495	-0.0439	-0.0418				
10	-0.0476	-0.0421	-0.0412	-0.0378	-0.0322	0.0058	0.0163
11		-0.0457	-0.0537	-0.0445	-0.0398	-0.0310	-0.0340

The EMAT technology for thickness measurement is a couplant free, accurate, and repeatable thickness measurement technique. The couplant variations or the orientation of the sensor does not affect the accuracy of the measurement. The other advantage of EMATs is the ability to generate strong shear horizontal waves that provide better time resolution due to the velocity of the wave mode that is approximately half of the conventional longitudinal wave from piezo sensors. MRUT is also recommended for quick screening of the tank wall for corrosion and wall loss. On tanks without insulation, MRUT could provide a quick assessment and identify areas of ID and OD corrosion at the bottom of the tank. Similarly, on tanks with insulation, MRUT might provide the inspection of a large area of the internal vessel by opening a small hole in the outer shell.

Because all EMAT sensors have some dead zone equivalent to a minimum of 1/8-inches depending upon excitation frequency and number of cycles in the excitation signal. One possible disadvantage of EMAT can be its measurement ability of the thin parts of a test piece. However, wherever multiple back wall responses are achieved outside the main bang (dead zone), a differential measurement algorithm along with advanced signal processing techniques can be used to achieve an accurate measurement of time.

6.5 3D Laser Scanning Metrology

The 3D laser scanner metrology method offers an alternative to the manual pit gauge measurement technique because it is an optical surface inspection technique that uses a combination of lasers and white-light technologies where multiple laser lines are projected in part while white-light devices project a light and shade a pattern. The scanning results are represented using freeform, unstructured 3D data, usually in the form of a point cloud or a triangular mesh. The images or scans are then brought into a common reference system where the data is merged into a complete model. This process, called alignment or registration, can be performed during the scan itself (dynamic referencing) or as a post-processing step [54, 55]. Once processed, the images/scans can be exported to Microsoft Excel for an inspector manual depth intervention.

To demonstrate this technology, a commercial, portable, metrology-grade 3D scanner was used to scan corrosion test panels reported in prior sections. The rated accuracy of the scanner used was up to 0.0009-inches with a measurement resolution of 0.0009-inches and a mesh resolution of 0.0039-inches. The scanning area capability measured 10.8-inch x 9.8-inch. The resolution of the scanner (minimum distance between two data points) can be adjusted based on different requirements/applications, and there is always a tradeoff on selecting higher and lower resolutions. A higher degree of details can be achieved using a higher resolution, but a higher resolution creates with a large data file size and requires extra computational power. The OEM recommendation is to choose half of the smallest flaw size value for the resolution. For this trial, the resolution of the scanner was set to 0.06-inches. The first step of the scanning process involved preparing the inspection surface for the scan and calibrating the scanner. A clean surface without any dirt, grease, or rust for the calibration was recommended. This method also required the use of reflective targets that are typically 0.25-inch diameter stickers or wire mesh applied randomly on the inspection surface. The spacing between targets was approximately 4 inches, but it can vary depending on different applications or purposes (Figure 40).

The second step of the scanning process was to acquire the data from the region of interest in the test area. Once the acquisition parameters were set, the scanner was held approximately 10 to 12 inches from the panel surface to start the data acquisition. The scanner was moved manually along the test piece to "paintbrush" the area of interest while validating the scan coverage. The 3D file was in STL format and Figure 41 through Figure 46 presents the results obtained from this trial.

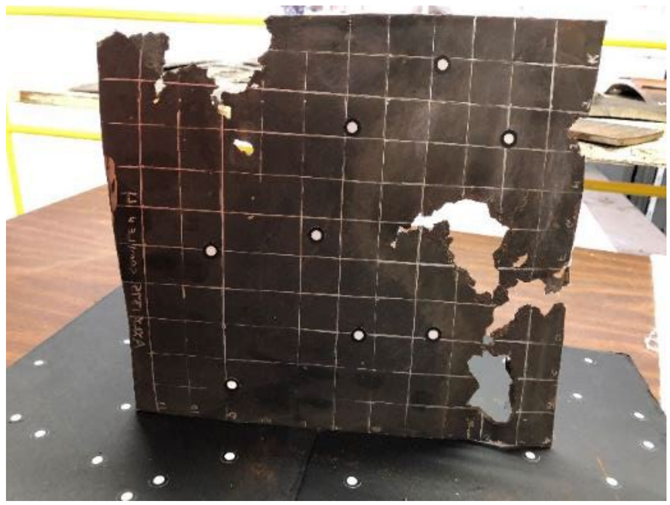

Figure 40. Placement of the reflective positioning targets for scanning

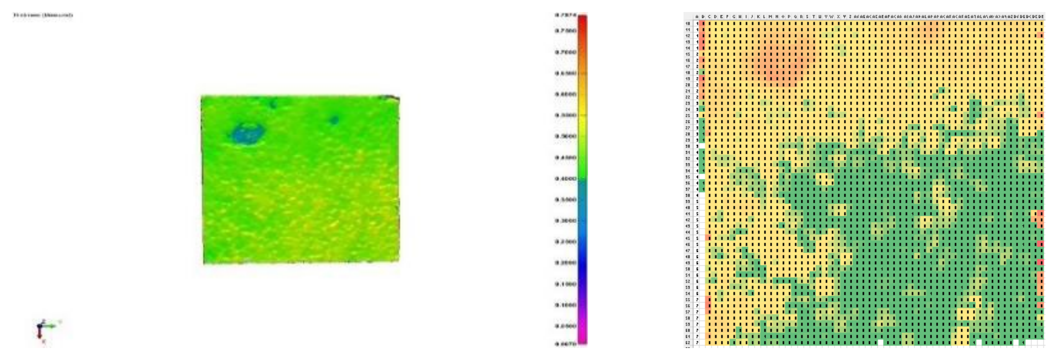

(a) (b)

Figure 41. 3D laser scanning result for corrosion test panel 1: (a) two-dimentional (2D) map; (b) Excel generated map with surface depth values

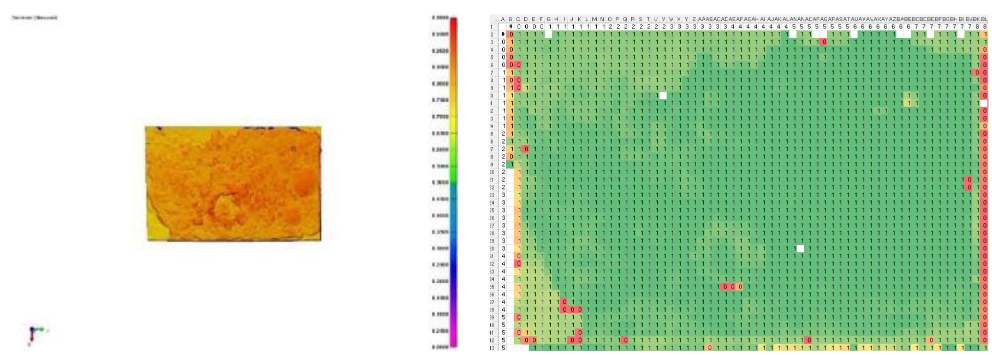

(a) (b)

Figure 42. 3D laser scanning result for corrosion test panel 2: (a) 2D map; (b) Excel generated map with surface depth values

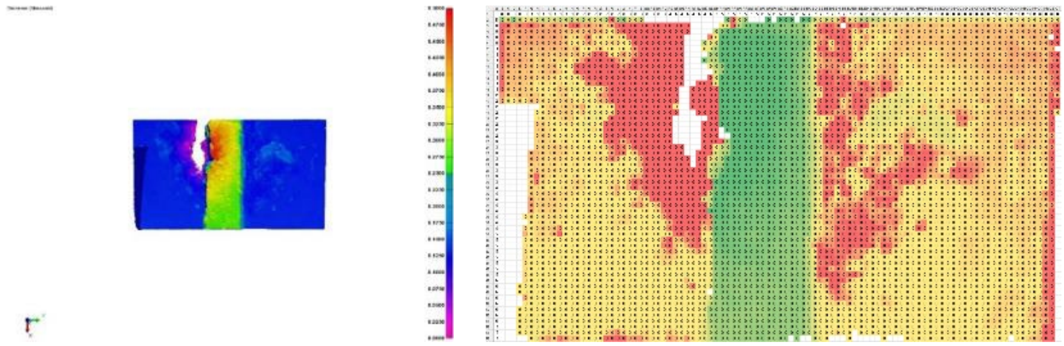

(a) (b)

Figure 43. 3D laser scanning result for corrosion test panel 3. (a) 2D map; (b) Excel generated map with surface depth values

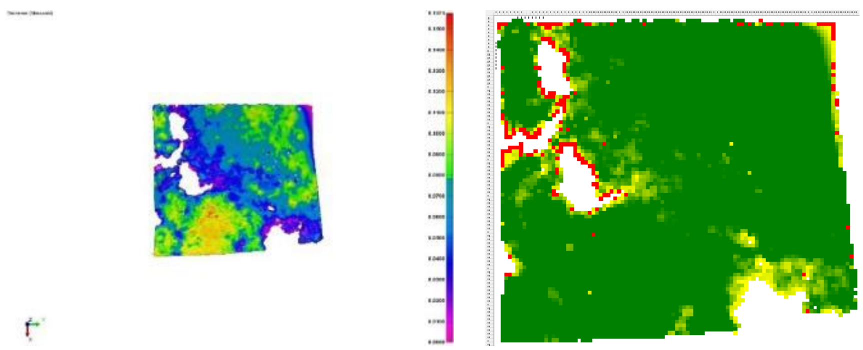

(a) (b)

Figure 44. 3D laser scanning result for corrosion test panel 4: (a) 2D map; (b) Excel generated map with surface depth values

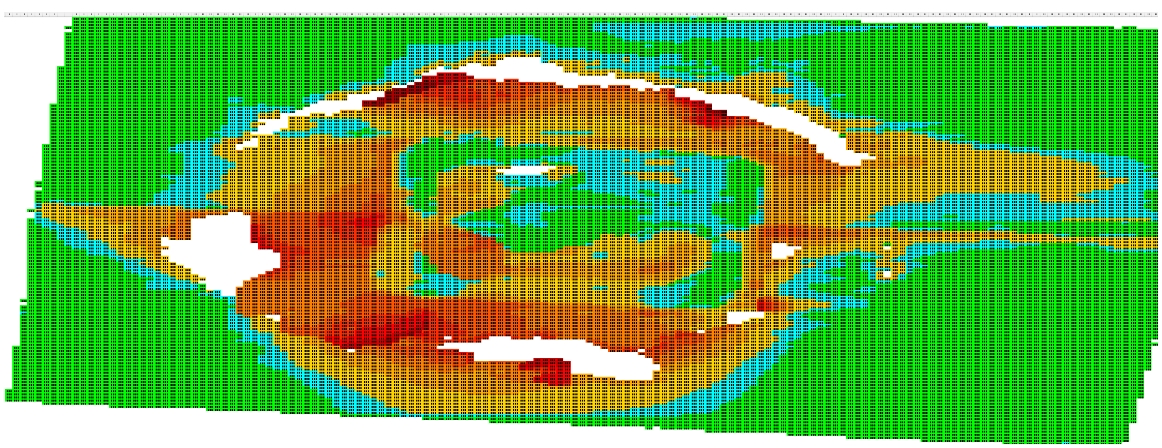

Figure 45. **3D laser scanning result for corrosion test panel 5 showing excel generated map with surface depth values**

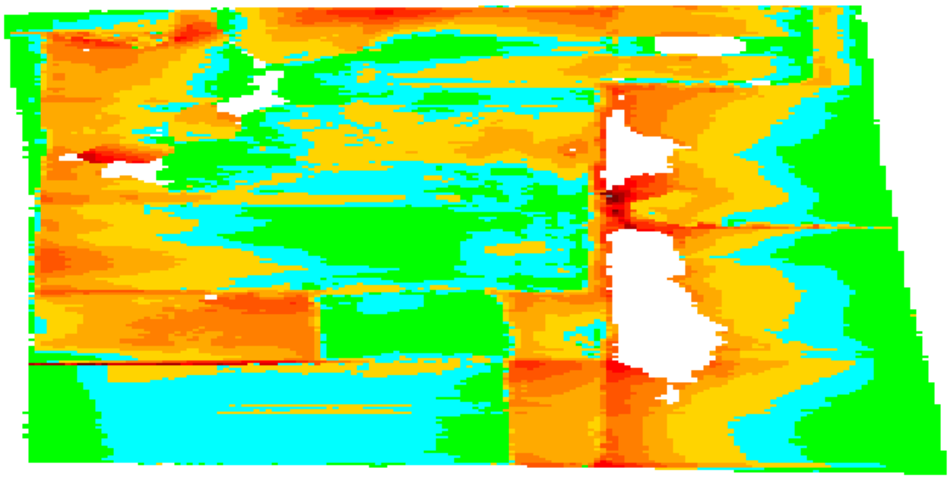

Figure 46. **3D laser scanning result for corrosion test panel 6 showing excel generated map with surface depth values**

The second set of trials was conducted on the simulated corrosion of MG plates. The damage detection threshold was set at 0.015-inches during post-processing. Figure 47 shows the detection results for the ID and OD surfaces of all six corrosion MG plates. For the most part, this technology was able to determine the simulated corrosion and pit maximum depth value, but there were instances when this technique was unable to determine smaller corrosion and pits, i.e., with depths ≤ 0.16-inches. The threshold can be adjusted lower to fit the needs of the user. For example, for the MGC-3 plate, flaw 3, an ID corrosion with max depth of 0.12, was not initially detected. By adjusting the threshold, however, the scanner was able to image flaw 3 and provide the max depth, a depth that was very close to the actual depth. Table 18 lists the details of the as-built simulated corrosion and pit depth sizes and compares these measurements with the 3D laser scanner approximated maximum depths measurements.

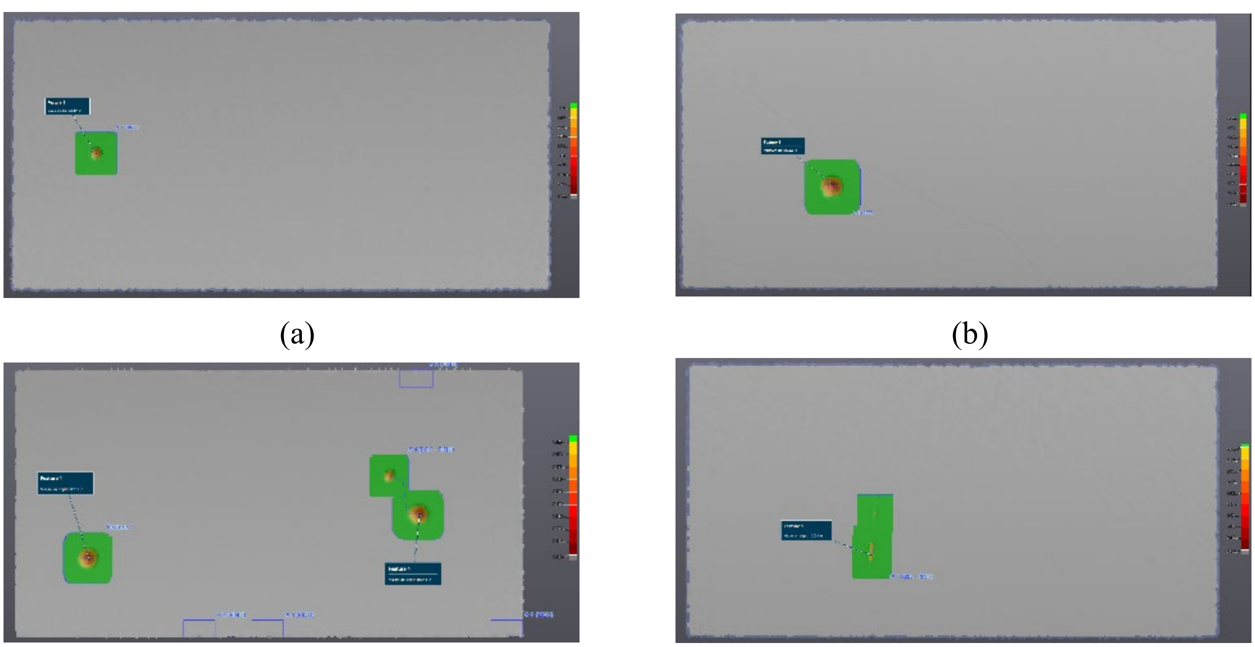

(a) (b)

(c) (d)

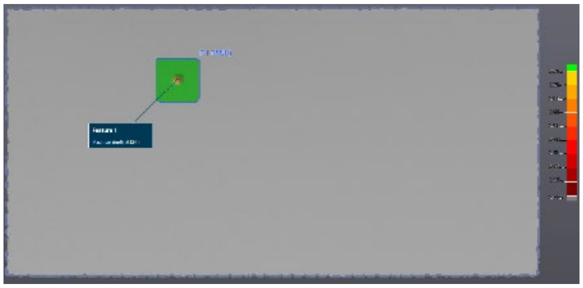

(e)

(f)

(g)

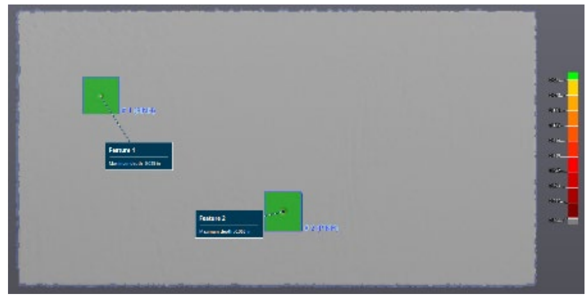

(h)

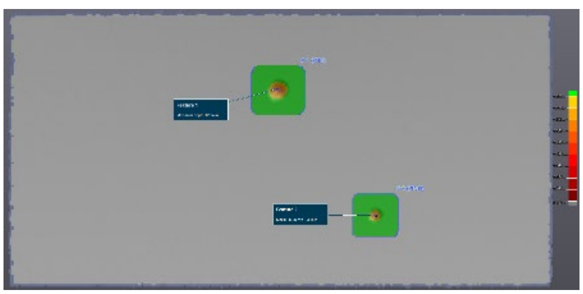

(i)

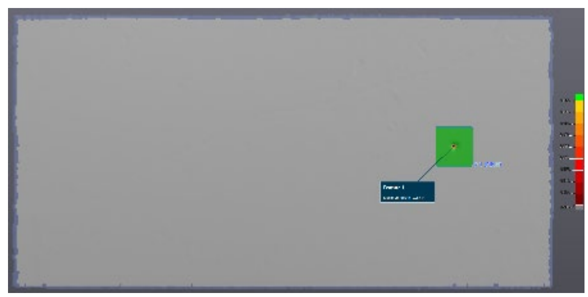

(j)

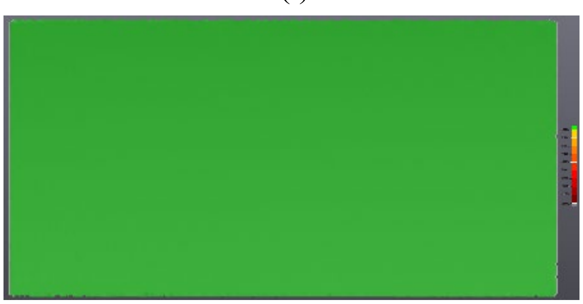

(k)

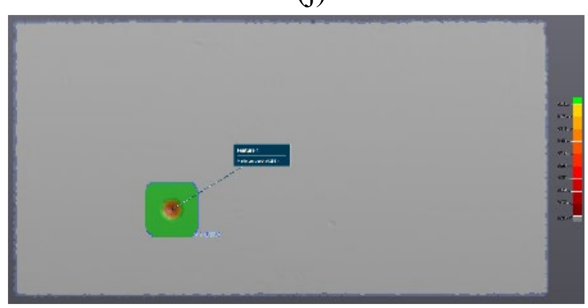

(l)

Figure 47. 3D laser scanning result for corrosion MG plates: (a) MGC-1 ID; (b) MGC-1 OD; (c) MGC-2 ID; (d) MGC-2 OD; (e) MGC-3 ID; (f) MGC-3 OD; (g) MGC-4 ID; (h) MGC-4 OD; (i) MGC-5 ID; (j) MGC-5 OD; (k) MGC-6 ID; (l) MGC-6 OD

Table 18. Comparison of the actual simulated corrosion and pit maximum pit depth value with the 3D laser scanning maximum depth value

MG Plates ID	Indication Types/ ID or OD	Simulated Corrosion/Pits Max. Depth Size [inch]	3D Laser Corrosion/Pits Max. Depth Size [inch]
MGC-1	Flaw 1 – Corrosion – OD	0.240	0.239
	Flaw 2 – Pit – ID	0.140	Not determined
	Flaw 3 – Corrosion - ID	0.170	0.161
MGC-2	Flaw 1 – Corrosion – ID	0.240	0.244
	Flaw 2 – Corrosion – ID	0.130	0.124
	Flaw 3 – Corrosion - ID	0.240	0.239
MGC-3	Flaw 1 – Corrosion – ID	0.240	0.242
	Flaw 2 – Corrosion – ID	0.020	Not determined
	Flaw 3 – Corrosion - ID	0.120	0.124
MGC-4	Flaw 1 – Pit – OD	0.060	0.035
	Flaw 2 – Corrosion – OD	0.130	0.063
	Flaw 3 – Corrosion – ID	0.120	0.120
MGC-5	Flaw 1 – Corrosion – ID	0.120	0.131
	Flaw 2 – Corrosion – ID	0.180	0.194
	Flaw 3 – Corrosion – OD	0.060	0.057
MGC-6	Flaw 1 – Corrosion – OD	0.020	Not determined
	Flaw 2 – Corrosion – OD	0.250	0.256
	Flaw 3 – Pit – OD	0.160	Not determined

The third set of trials was conducted on the DOT-117 corrosion MG reflector plates. These plates had FBHs with different diameters drilled at different depths. In addition, there were cases where FBHs were drilled in the existing FBHs. These plates demonstrate the resolution and sensitivity of the inspection methods explored. Figure 48 shows the 3D laser scanner results for these plates, once again correlating fairly well with the engineering drawings presented in prior sections. Table 19 through Table 21 show the quantitative depth sizing measurements that were taken using these reflector plates. Once again, there were instances this technique was unable to determine extremely smaller FBHs.

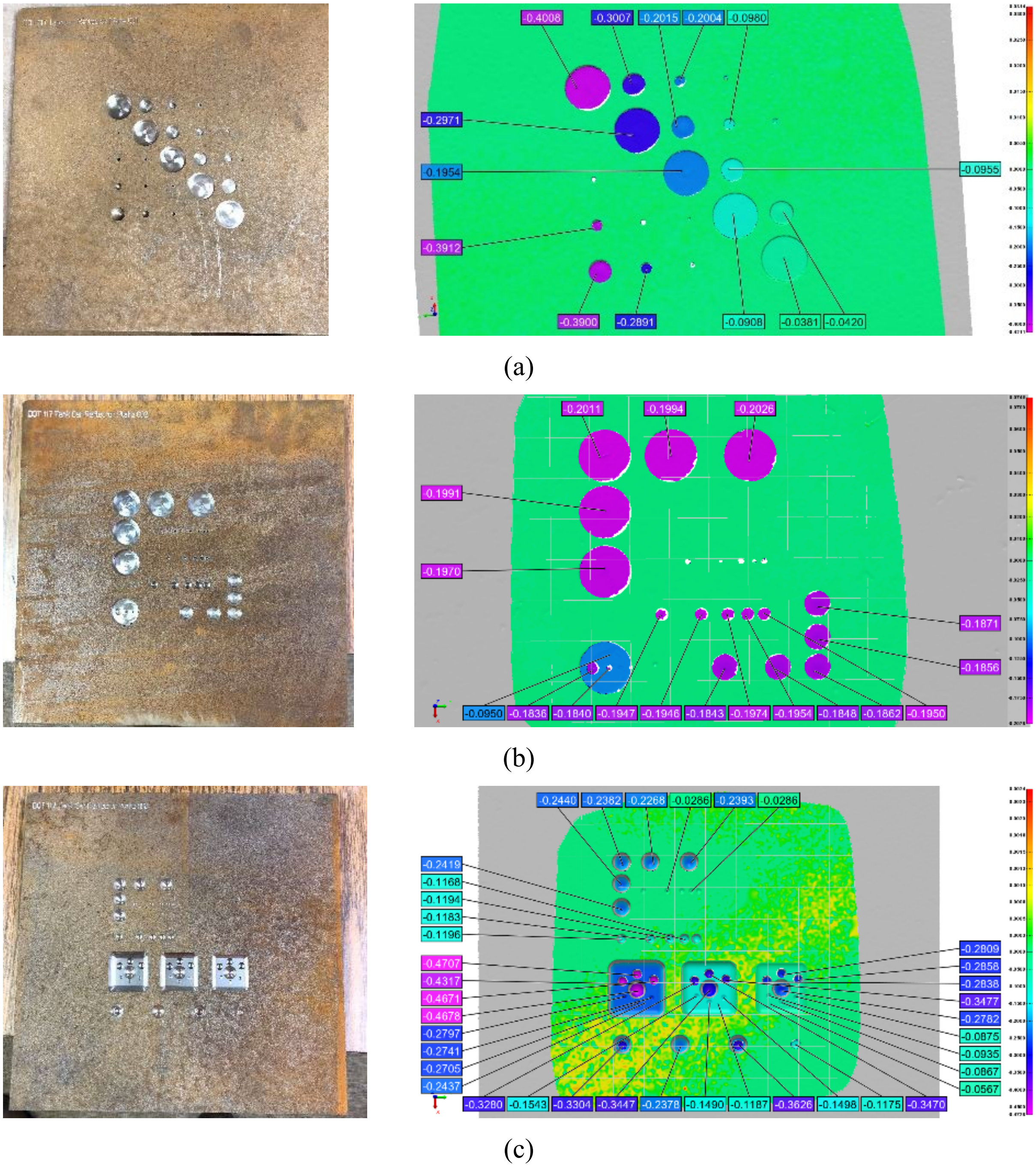

Figure 48. 3D laser scanning results for corrosion reflector plates: (a) plate 001; (b) plate 002; (c) plate 003

Table 19. Comparison of the actual reflector depth value with the 3D laser scanning maximum depth value in DOT-117 tank car corrosion reflector plate 001

FGH Dia. [inch]	Actual Max. Depth [inch]	Measured Max. Depth [inch]	Difference
1.000	0.40	0.4233	-0.0233
	0.30	0.3497	-0.0497
	0.20	0.2271	-0.0271
	0.10	0.1121	-0.0121
	0.05	0.0423	0.0077
0.500	0.40	0.4074	-0.0074
	0.30	0.3154	-0.0154
	0.20	0.2196	-0.0196
	0.10	0.1038	-0.0038
	0.05	0.0495	0.0005
0.250	0.40	0.4267	-0.0267
	0.30	0.3162	-0.0162
	0.20	0.2261	-0.0261
	0.10	0.1143	-0.0143
	0.05	Not detected	N/A
0.130	0.40	0.1392	0.2608
	0.30	0.1360	0.1640
	0.20	0.1300	0.0700
	0.10	0.1391	-0.0391
	0.05	0.0672	-0.0172
0.060	0.40	0.0634	0.3366
	0.30	0.0182	0.2818
	0.20	0.1099	0.0901

Table 20. Comparison of the actual reflector depth value with the 3D laser scanning maximum depth value in DOT-117 tank car corrosion reflector plate 002

FGH Dia. [inch]	Hole #	Actual Max. Depth [inch]	Measured Max. Depth [inch]	Difference
1.000	1	0.20	0.2263	-0.0233
	2	0.20	0.2387	-0.0387
	3	0.20	0.2511	-0.0511
	4	0.20	0.2234	-0.0234
	5	0.20	0.2033	-0.0053
	6	0.10	0.1033	-0.0033
0.500	1	0.20	0.1033	-0.0033
	2	0.20	0.2213	-0.0213
	3	0.20	0.2079	-0.0079
	4	0.20	0.1963	-0.0037
	5	0.20	0.1940	0.0060
0.250	1	0.20	0.2093	-0.0093
	2	0.20	0.2291	-0.0291
	3	0.20	0.2080	-0.0080
	4	0.20	0.2278	-0.0278
	5	0.20	0.2453	-0.0453
	6	0.19	0.1988	-0.0088
0.130	1	0.20	0.0814	
	2	0.20	0.0990	
	3	0.20	0.0707	
	4	0.20	0.0839	
	5	0.20	0.1582	
	6	0.20	0.2024	
0.060	1	0.20	Not Detected	N/A
	2	0.20	Not Detected	N/A
	3	0.20	Not Detected	N/A
	4	0.20	0.1165	-0.0835
	5	0.20	Not Detected	N/A

FGH Dia. [inch]	Hole #	Actual Max. Depth [inch]	Measured Max. Depth [inch]	Difference
	6	0.19	Not Detected	N/A
	7	0.19	Not Detected	N/A
	8	0.39	Not Detected	N/A
	9	0.19	Not Detected	N/A

Table 21. Comparison of the actual reflector depth value with the 3D laser scanning maximum depth value in DOT-117 tank car corrosion reflector plate 003

FGH Dia. [inch]	Hole #	Actual Max. Depth [inch]	Measured Max. Depth [inch]	Difference
0.500	1	0.25	0.2382	0.0118
	2	0.25	0.2268	0.0232
	3	0.25	0.2393	0.0107
	4	0.25	0.2440	0.0060
	5	0.25	0.2419	0.0081
	6	0.40	0.4709	-0.0709
	7	0.28	0.3473	-0.0723
	8	0.21	0.2849	-0.0729
	9	0.22	0.2878	-0.0678
	10	0.25	0.2378	0.0122
	11	0.25	0.3176	-0.0676
0.250	1	0.13	0.1196	0.0054
	2	0.13	0.1183	0.0067
	3	0.13	0.1194	0.0056
	4	0.13	0.1168	0.0082
	5	0.13	0.1201	0.0049
	6	0.49	0.4317	0.0533
	7	0.49	0.4707	0.0143
	8	0.49	0.4671	0.0179
	9	0.37	0.3280	0.0370
	10	0.37	0.3470	0.0180
	11	0.37	0.3477	0.0173

FGH Dia. [inch]	Hole #	Actual Max. Depth [inch]	Measured Max. Depth [inch]	Difference
	12	0.30	0.2838	0.0112
	13	0.30	0.2809	0.0141
	14	0.30	0.2858	0.0092
	15	0.34	0.3304	0.0116
	16	0.34	Not Detected	N/A
	17	0.13	0.1175	0.0075
0.130	1	0.06	0.0286	0.0339
	2	0.06	0.0290	0.0335
	3	0.06	0.0293	0.0332
	4	0.06	0.0286	0.0339
	5	0.06	0.0287	0.0338
	6	0.35	0.2797	0.0703
	7	0.35	0.2705	0.0795
	8	0.35	0.2741	0.0759
	9	0.23	0.1543	0.0757
	10	0.23	0.1490	0.0810
	11	0.23	0.1498	0.0802
	12	0.16	0.0935	0.0665
	13	0.16	0.0867	0.0733
	14	0.16	0.0875	0.0725
	15	0.39	0.3626	0.0244
Square Cut	1	0.25	0.2457	0.0043
	2	0.13	0.1213	0.0087
	3	0.06	0.0605	-0.0005

Finally, a separate demonstration was conducted in the ID of the actual tank car to demonstrate the capability of the scanner (Figure 49).

Figure 49. Tank car scanned area

The scan took the follow amount of time to complete:

- Setup scanner and computer: 3 minutes
- Drawing positioning targets: 5 minutes using two people (8 feet x 8 feet surface)
  0 minutes if using wire frame
- Scanning time: 7 minutes
- Saving data: 1 minute
- Report generation: 15 seconds

In total to scan the 8-ft x 8-foot section, it roughly took 16 minutes.

The resulting scan, shown in Figure 50 and in Excel form in Figure 51, shows no major damage. Some very fine waviness was measured in some areas. The blue area represented the deepest point at approximately 0.03 inches.

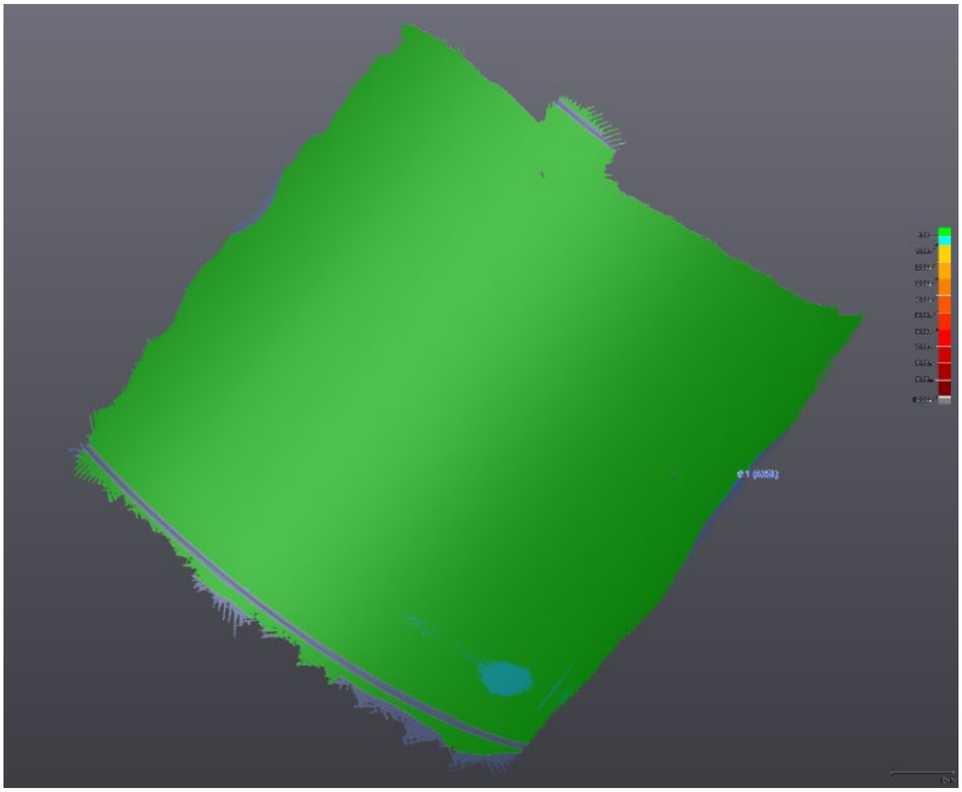

Figure 50. 3D results for the tank car section

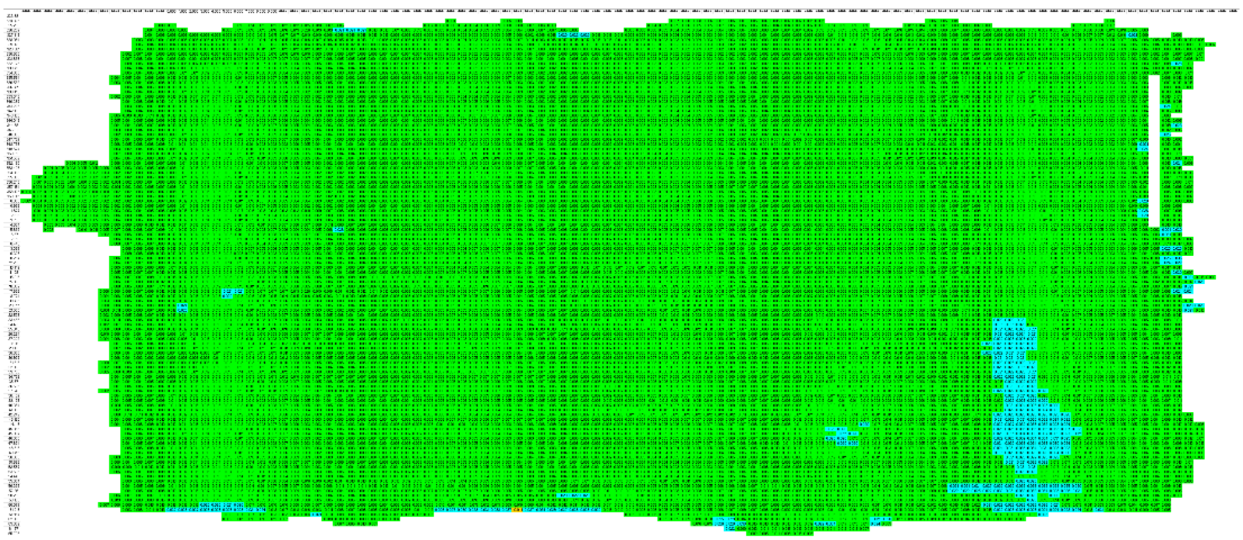

Figure 51. Exported depth map for the tank car section

6.6 Quantitative Corrosion/Pit Sizing Analysis

The final set of research consisted of visual testing (VT), UTT, and PAUT methods for sizing corrosion and pits in six corrosion MG plates. Figure 52(b–c) shows the test setup used.

(a)

(b)

(c)

Figure 52. NDE method setup for corrosion MG plates defect sizing analysis: (a) VT; (b) UTT; (c) PAUT

The corrosion defects on each MG panel were evaluated by each NDE method. The evaluation of each notch was classified into one of the following four groups:

- TP = true positive: the defect was indicated where it was present (hit)
- FN = false negative: the defect was not indicated where it was present (miss)

- TN = true negative: the defect was not indicated where it was not present
- FP = false positive: the defect was indicated where it was not present (false alarm)

Each different NDE method evaluated 18 defects and calculated the probability of hits (POH). The number of correct evaluations, true positive and true negative, was divided by the total number of notches evaluated. Table 22 shows the probability of correct hits grouped by NDE method as well as the full results for each of the three NDE evaluation result categories. In each possible defect locations, they created no chance of a true negative or false positive.

Table 22. POH grouped by NDE method

NDE Methods	True Positive	True Negative	False Positive	False Negative	POH
VT	18	-	-	-	100%
UT	17	-	-	1	94%
PAUT	14	-	-	4	78%

6.6.1 Analysis of Corrosion Defect Size Difference

Figure 53 shows the overall measurement results from each corrosion flaw displayed as the difference from the flaw design length grouped by NDE methods. Positive differences indicate the measured crack was longer than the design drawing of the notch indicated, while a negative difference indicates the measured crack was shorter than the design. VT UT methods had means close to zero difference as compared to PAUT, the method that had the median the farthest away from zero difference. Ninety-three percent of the 49 length measurements were within 0.19 inches of the design length of the notch. Seventy-five percent of the measurements were within 0.11 inches of the design length.

Figure 54 shows the overall measurement results displayed as the difference from the flaw design width grouped by NDE methods. The results are similar to those in the previous figure. This similarity is expected due to the circular nature of the flaws. Again, the PAUT method's median is the farthest away from zero difference.

Figure 55 shows the measurement results displayed as the difference from the notch design depth grouped by NDE methods. The depths were much shorter compared to the length or width of the manufactured flaw so the proximity of the depth difference for UT and PAUT is closer to zero.

Figure 56 combines the length and width results, but then separates the measures based on which side of the panel the defect occurred. The largest visible difference in medians is for PAUT when measuring ID versus outside OD.

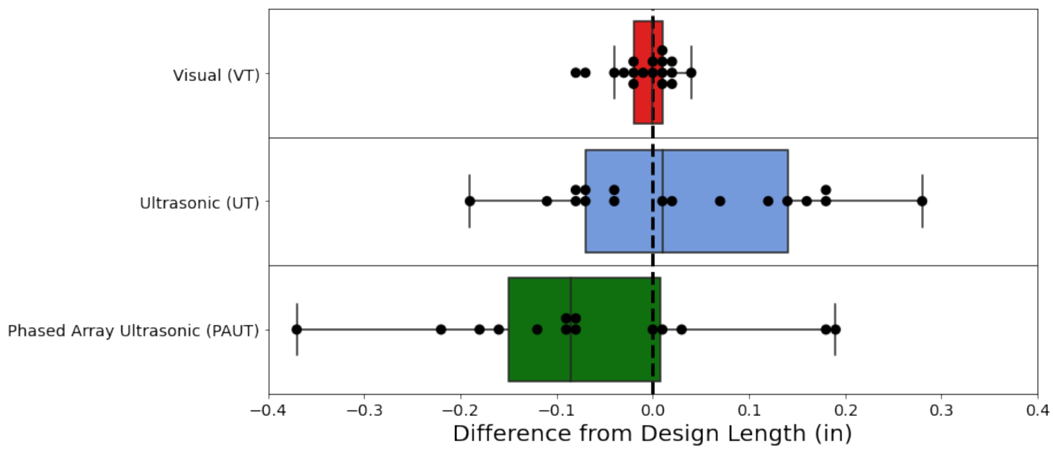

Figure 53. Boxplots and individual points for differences from design length

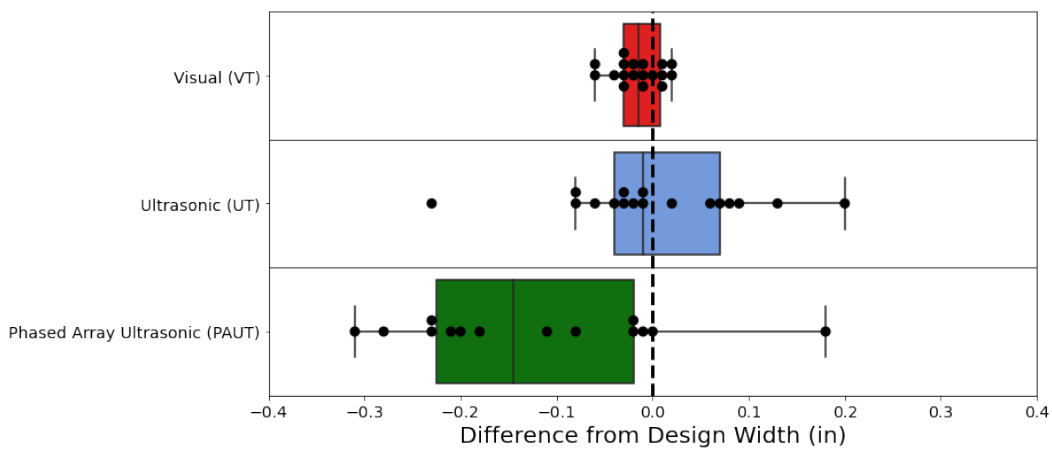

Figure 54. Boxplots and individual points for differences from design width

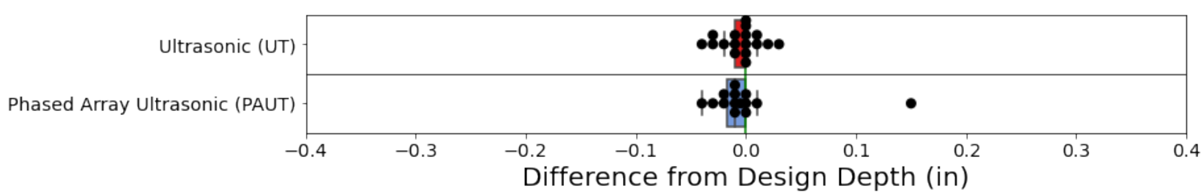

Figure 55. Boxplots and individual points for differences from design depths

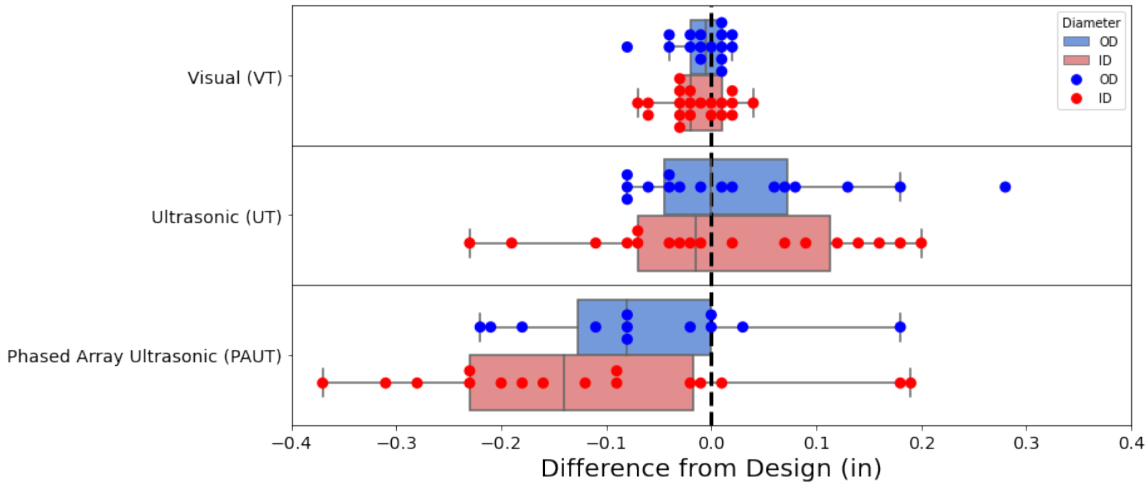

Figure 56. Boxplots and individual points for difference from design—length and width combined

7. Conclusion

Corrosion poses challenges that can affect the safety and structural integrity of tank cars. Effective corrosion monitoring, prevention, and prediction techniques can help extend the life of a tank car that usually carries Class 3 flammable liquids and other cryogenic liquids. No single NDE method is suitable for all forms of corrosion. The design of jacketed cars poses additional challenges to corrosion inspection, often requiring cutting the jacket to inspect the tank car shell. Since corrosion is not localized, a point measurement technique is not reliable as it may not provide us with a realistic detail for other parts of the tank car structure. To investigate possible NDE inspection solutions for tank cars, preparing several tank cars panels with real corrosion defect as well as simulated corrosion defects took place. Then, some of the advanced NDE methods were explored as a part of this study, including PAUT, EMATs, backscatter X-ray imaging, and 3D laser scanning metrology methods. While these NDE methods demonstrated good feasibility, other efforts should be considered and pursued in exploring each of these NDE methods as well as other NDE methods in a more systematic way that will allow a better understanding of the capabilities and limitations of each of these NDE methods. Future efforts should also consider building more test panels for the corrosion NDE demonstration.

8. References

[1] Hitt, R., "The Car Builders' Dictionary," The Master Car Builders' Association, New York, NY, 1903.

[2] *Code of Federal Regulation,* Title 49 CFR Parts 179–180 Chapter I Subchater C–Hazardous Materials Regulations, Washington, DC: U.S. Department of Transportation, 2020.

[3] Association of American Railroads, *Manual of Standards and Recommended Practices*, *(MSRP), Section C, Part III, Specifications for Tank Cars, M-*1002, Washington, DC, 2022.

[4] Association of American Railroads, *Manual of Standards and Recommended Practices*, Section C, Part II, Volume 1 -Specification for Design, Fabrication, and Construction of Freight Cars, M-1001Washington, DC, 2022.

[5] Railinc, "UMLER®: Universal Machine Language Equipment Register."

[6] Bureau of Transportation Statistics, *Fleet Composition of Rail Tank Cars Carrying Flammable Liquids: 2021 Report*, Washington, DC: U.S. Department of Transportation, 2021.

[7] Bharatiya, U., Gal, P., Agrawal, A., Shah, M., and Sircar, A., "Effect of Corrosion on Crude Oil and Natural Gas Pipeline with Emphasis on Prevention by Ecofriendly Corrosion Inhibitors: A Comprehensive Review," *Journal of Bio- and Tribo-Corrosion*, *5*(2), p. 35, 2019, doi: 10.1007/s40735-019-0225-9.

[8] BDM Federal, Inc., "Corrosion Detection Technologies Sector Study," Washington, DC: North American Technology and Industrial Base Organization, 1998.

[9] Okonkwo, P. and Mohamed, A. M. A., "Erosion-Corrosion in Oil and Gas Industry: A Review," *International Journal of Metallurgical & Materials Science and Engineering (IJMMSE)*, Doha, Qatar: Center for Advanced Materials, *4*(3), pp. 7–28, 2014.

[10] Groysman A., "Corrosion Problems and Solutions in Oil Refining and Petrochemical Industry," *Koroze a ochrana materialu*, *61*(3), pp. 100–117, 2017, doi:10.1515/kom-2017-0013.

[11] Feng, Y., Yang, Y., and Huang, B., "Corrosion Analysis and Remaining Useful Life Prediction for Storage Tank Bottom," *International Journal of Advanced Robotic Systems, 16*(5), p. 1729881419877051, 2019, doi: 10.1177/1729881419877051.

[12] Kermani, M. B. and Harrop, D., "The Impact of Corrosion on the Oil and Gas Industry," *SPE Production & Operations*, *11*(03), pp. 186–190, 1996.

[13] Berntsen, T., Seiersten, M., and Hemmingsen, T., "Effect of $FeCO_3$ Supersaturation and Carbide Exposure on the CO_2 Corrosion Rate of Carbon Steel," *Proceedings of the Nace International Corrosion 2011 Conference & Expo*, *69*(6), pp. 601–613, 2013.

[14] Singh, R., "Material Selection for Sour Service Environment," *Pipeline & Gas Journal*, *237*(2), 2010.

[15] Stahle, R. W., Hochmann, J., McCright, R. D., Slater, J. E., and Shatynski, S. R., "Stress Corrosion Cracking and Hydrogen Embrittlement of Iron Base Alloys," *Journal of The Electrochemical Society*, *126*(5), pp. 215C–215C, 1979, doi: 10.1149/1.2129122.

[16] Hardie, D., Charles, E. A., and Lopez, A. H., "Hydrogen embrittlement of high strength pipeline steels," *Corrosion Science,* 48(12), pp. 4378–4385, 2006.

[17] Silva, S. C., Silva, A. B., and Ponciano Gomes, J. A. C., "Hydrogen embrittlement of API 5L X65 pipeline steel in CO_2 containing low H_2S concentration environment," *Engineering Failure Analysis,* vol. 120, p. 105081, 2021.

[18] Kvarekvål, J., and Moloney, J., "6 - Sour Corrosion," in *Trends in Oil and Gas Corrosion Research and Technologies*, A. M. El-Sherik Ed. Boston: Woodhead Publishing, pp. 113–147, 2017.

[19] Lebozec, N., Persson, D., Thierry, D., and Axelsen, S., "Effect of Climatic Parameters on Filiform Corrosion of Coated Aluminum Alloys," *Corrosion,* vol. 60, pp. 584–593, 2004, doi: 10.5006/1.3287763.

[20] Spraul, J. R., "Testing Tank Car Linings," *Corrosion - The Journal of Science & Engineering, 10*(8), pp. 243–247, 1954.

[21] Miksic, B. M., Furman, A. Y., and Kharshan, M. A., "Effectiveness Of The Corrosion Inhibitors For The Petroleum Industry Under Various Flow Conditions," in *CORROSION 2009*, Paper No. NACE-09573, 2009.

[22] Sastri, V. S., *Corrosion Inhibitors: Principles and Applications*. Chichester: New York: Wiley (in English), 1998.

[23] Yang, L., *Techniques for Corrosion Monitoring*. Elsevier Science, 2020.

[24] Komorowski, J. P., Bellinger, N. C., Gould, R. W., and Reynolds, R., "Quantification of Corrosion in Aircraft Structures with Double Pass Retroreflection," *Canadian Aeronautics and Space Journal, 42*(2), pp. 76–82, Quebec, Montreal, 1996.

[25] Forsyth, D. S., Marincak, A., and Komorowski, J. P., "Edge of Light: A New Enhanced Optical NDI Technique," *CASJ, 43*(4), pp. 231–235, 1997.

[26] Prewitt, T. J., "Application of 3D Metrology Technology in Inspection, Corrosion Mapping, and Failure Analysis," in *CORROSION 2016*, Report No. NACE-2016-7672, British Columbia, Canada, 2016.

[27] Abu-Four, M. A., and Al-Salahi, I., "Corrosion Under Insulation Inspection Challenge," *Proceedings for the 26th ASNT Research Symposium*, Jacksonville, FL, 2017.

[28] Mardaninejad, R., and Safizadeh, M. S., "Gas Pipeline Corrosion Mapping Through Coating Using Pulsed Eddy Current Technique," *Russian Journal of Nondestructive Testing*, *55*(11), pp. 858–867, 2019, doi: 10.1134/S1061830919110068.

[29] Thome, D., Fitzpatrick, G., Skaugset, R., and Shih, W., "Aircraft Corrosion and Crack Inspection using Advanced Magneto-optic Imaging Technology," in *Nondestructive Evaluation Techniques for Aging Infrastructure and Manufacturing*, 1996, vol. 2945.

[30] Safizadeh, M. S., Lepine, B. Forsyth, A., D. S., and Fahr, A., "Time-Frequency Analysis of Pulsed Eddy Current Signals," *Journal of Nondestructive Evaluation*, *20*(2), pp. 73–86, 2001, doi: 10.1023/A:1012244208475.

[31] Cheng, W., "Pulsed Eddy Current Testing of Carbon Steel Pipe's Wall-thinning Through Insulation and Cladding," *Journal of Nondestructive Evaluation*, *31*(3), pp. 215–224, 2012, doi: 10.1007/s10921-012-0137-9.

[32] Goldfine, N., Dunford, T., Washabaugh, A., Chaplan, S., and Diaz, K., "MWM-Array and MR-MWM-Array Eddy Current Testing for Piping and Vessels," in *ASNT Research Symposium*, doi: 10.32548/RS.2019.010, Los Angeles, CA, 2019.

[33] Hirao, M., and Ogi, H., "An SH-Wave EMAT Technique for Gas Pipeline Inspection," *NDT & E International*, *32*(3), pp. 127–132, 1999.

[34] Nagy, P. B., Simonetti, F., and Instanes, G., "Corrosion and Erosion Monitoring in Plates and Pipes Using Constant Group Velocity Lamb Wave Inspection," *Ultrasonics, 54*(7), pp. 1832–1841, 2014, doi: https://doi.org/10.1016/j.ultras.2014.01.07.

[35] García, V., Boyero, C., and Garrido, J. A. J., "Corrosion Detection Under Pipe Supports Using EMAT Medium Range Guided Waves," *Proceedings of the 19th World Conference on Non-Destructive Testing*, Munich, Germany, 2016.

[36] Bubenik, T., "7 - Electromagnetic Methods for Detecting Corrosion in Underground Pipelines: Magnetic Flux Leakage (MFL)," in *Underground Pipeline Corrosion*, M. E. Orazem Ed.: Woodhead Publishing, 2014, pp. 215–226.

[37] Peng, X., Anyaoha, U., Liu, Z., and Tsukada, K., "Analysis of Magnetic-Flux Leakage (MFL) Data for Pipeline Corrosion Assessment," *IEEE Transactions on Magnetics*, *56*(6), pp. 1–15, 2020, doi: 10.1109/TMAG.2020.2981450.

[38] Doshvarpassand, S., Wu, C., and Wang, X., "An Overview of Corrosion Defect Characterization Using Active Infrared Thermography," *Infrared Physics & Technology*, vol. 96, pp. 366–389, 2019.

[39] Jönsson, M., Rendahl, B., and Annergren, I., "The Use of Infrared Thermography in the Corrosion Science Area," *Materials and Corrosion, 61*(11), pp. 961–965, 2010.

[40] Kharkovsky, S., and Zoughi, R., "Millimeter Wave Nondestructive Evaluation of Corrosion Under Paint in Steel Structures," *AIP Conference Proceedings*, *820*(1), pp. 1277–1283, 2006, doi: 10.1063/1.2184671.

[41] Kharkovsky, S., and Zoughi, R., "Microwave and millimeter wave nondestructive testing and evaluation - overview and recent advances," *IEEE Instrumentation & Measurement Magazine, 10*(2), pp. 26–38, 2007, doi: 10.1109/MIM.2007.364985.

[42] Anastasi, R. et al., "Terahertz NDE Application for Corrosion Detection and Evaluation Under Shuttle Tiles," in *SPIE Smart Structures and Materials + Nondestructive Evaluation and Health Monitoring*, 2007, vol. 6531.

[43] Jamshidi, V., and Davarnejad, R., "Simulation of Corrosion Detection Inside Wellbore by X-ray Backscatter Radiography," *Applied Radiation and Isotopes,* vol. 145, pp. 116–119, 2019.

[44] Dunn, W. L., and Yacout, A. M., "Corrosion Detection in Aircraft by X-ray Backscatter Methods," *Applied Radiation and Isotopes, 53*(4), pp. 625–632, 2000.

[45] Brown, W. H., "Using ILI Pigs to Establish Pipeline Corrosion Rates - Case Histories," in *CORROSION 99*, 1999, Report No. NACE-99523.

[46] Bondurant, P., and Nino, G., *Development of EMAT Sensors for Corrosion Mapping of UNGP Using ILI Tools*, Washington, DC: U.S. Department of Transportation, Pipeline and Hazardous Materials Safety Administration, 2019.

[47] Afzal, M., and Udpa, S., "Advanced Signal Processing of Magnetic Flux Leakage Data Obtained from Seamless Gas Pipeline," *NDT & E International*, *35*(7), pp. 449–457, 2002.

[48] Eltai, E. O., Musharavati, F., and Mahdi, E.-s., "Severity of Corrosion Under Insulation (CUI) to Structures and Strategies to Detect It," *Corrosion Reviews*, *37*(6), pp. 553–564, 2019, doi:10.1515/corrrev-2018-0102.

[49] Tsai, Y.-H., Wang, J., Chien, W.-T., Wei, C.-Y., Wang, X., and Hsieh, S.-H., "A BIM-based Approach for Predicting Corrosion Under Insulation," *Automation in Construction*, vol. 107, p. 102923, 2019.

[50] Shedlock, D., Edwards, T., and Toh, C., "X-Ray Backscatter Imaging for Aerospace Application," *Proceedings of the 37th Annual Review of Progress in Quantitative Nondestructive Evaluation (QNDE)*, San Diego, CA, 2011 Jul 18–23 2010, *1335*(1), in AIP Conference Proceedings, 2011, pp. 509–516, doi: 10.1063/1.3591894.

[51] Stokes, J. A., et al., "Some New Applications of Collimated Photon Scattering for Nondestructive Examination," *Nuclear Instruments and Methods in Physics Research*, *193*(1–2), pp. 261–267, 1982.

[52] Lawson, L., "Compton X-ray Backscatter Depth Profilometry for Aircraft Corrosion Inspection," *Materials Evaluation*, *53*(8), pp. 936–941, 1995.

[53] Hirao, M., and Ogi, H., *Electromagnetic Acoustic Transducers - Noncontacting Ultrasonic Measurements using EMATs*, 2nd ed. Japan: Springer, 2017.

[54] Allard, P.-H., Mony, C., and Beaumont, J., "Pipeline External Corrosion Analysis Using a 3D Laser Scanner," *Proceedings of the The NDT in Canada 2013 Conference*, Calgary, Alberta, 2013.

[55] Allard, P.-H., "Differentiation of 3D Scanners and Their Positioning Method When Applied to Pipeline Integrity," *Proceedings of the 11th European Conference on Non-Destructive Testing (ECND 2014)*, Prague, Czech Republic, Oct 6–11, 2014.

Abbreviations and Acronyms

Abbreviations	Definitions
AAR	Association of American Railroads
BW	Butt Weld
CO_2	Carbon Dioxide
CFR	Code of Federal Regulations
CUI	Corrosion Under Insulation
EMAT	Electro Magnetic Acoustic Transducer
FRA	Federal Railroad Administrative
FW	Fillet Weld
FAST Act	Fixing America's Surface Transportation Act
FBH	Flat Bottom Hole
HazMat	Hazardous Materials
HMR	Hazardous Materials Regulations
H_2S	Hydrogen Sulfide
IRT	Infrared Thermography
ILI	In-Line Inspection
ILM	In-Line Monitoring
ID	Inner Diameter
ICC	Interstate Commerce Commission
LRUT	Long-Range Ultrasonic Testing
MFL	Magnetic Flux Leakage
MSRP	Manual of Standards and Recommended Practices
MG	Master Gauge
MRUT	Medium-Range Ultrasonic Testing
NACE	National Association of Corrosion Engineers
NDE	Nondestructive Evaluation
OEM	Original Equipment Manufacturers
OD	Outer Diameter
PAUT	Phased Array Ultrasonic Testing
Pigs	Pipeline Inspection Gauges

Abbreviations	Definitions
POD	Probability of Detection
POH	Probability of Hit (Number of Hits /Total Number of Trials)
RT	Radiographic Testing
SH	Shear Horizontal
3D	Three-dimensional
TOF	Time of Flight
TC	Transport Canada
TTC	Transportation Technology Center (the site)
TTCI	Transportation Technology Center, Inc. (the company)
2D	Two-dimensional
DOT	U.S. Department of Transportation
UT	Ultrasonic Testing
UTT	Utrasonic Thickness
VT	Visual Testing